Celestial Mech Dyn Astr (2007) 99:261–292
DOI 10.1007/s10569-007-9099-0

ORIGINAL ARTICLE

Long-term evolution of orbits about a precessing oblate planet: 3. A semianalytical and a purely numerical approach

Pini Gurfil · Valéry Lainey · Michael Efroimsky

Received: 12 January 2006 / Revised: 31 July 2007 / Accepted: 14 September 2007 /
Published online: 21 November 2007

Abstract Construction of an accurate theory of orbits about a precessing and nutating oblate planet, in terms of osculating elements defined in a frame associated with the equator of date, was started in Efroimsky and Goldreich (2004) and Efroimsky (2004, 2005, 2006a, b). Here we continue this line of research by combining that analytical machinery with numerical tools. Our model includes three factors: the J_2 of the planet, its nonuniform equinoctial precession described by the Colombo formalism, and the gravitational pull of the Sun. This semianalytical and seminumerical theory, based on the Lagrange planetary equations for the Keplerian elements, is then applied to Deimos on very long time scales (up to 1 billion years). In parallel with the said semianalytical theory for the Keplerian elements defined in the co-precessing equatorial frame, we have also carried out a completely independent, purely numerical, integration in a quasi-inertial Cartesian frame. The results agree to within fractions of a percent, thus demonstrating the applicability of our semianalytical model over long timescales. Another goal of this work was to make an independent check of whether the equinoctial-precession variations predicted for a rigid Mars by the Colombo model could

We use the term "precession" in its general meaning, which includes any change of the instantaneous spin axis. So generally defined precession embraces the entire spectrum of spin-axis variations—from the polar wander and nutations through the Chandler wobble through the equinoctial precession.

P. Gurfil
Faculty of Aerospace Engineering, Technion, Haifa 32000, Israel
e-mail: pgurfil@technion.ac.il

V. Lainey
IMCCE/Observatoire de Paris, UMR 8028 du CNRS, 77 Avenue Denfert-Rochereau,
Paris 75014, France
e-mail: Valery.Lainey@imcce.fr

V. Lainey
Observatoire Royal de Belgique, Avenue Circulaire 3, Brussels 1180, Belgium

M. Efroimsky (✉)
US Naval Observatory, Washington, DC 20392, USA
e-mail: me@usno.navy.mil

have been sufficient to repel its moons away from the equator. An answer to this question, in combination with our knowledge of the current position of Phobos and Deimos, will help us to understand whether the Martian obliquity could have undergone the large changes ensuing from the said model (Ward 1973; Touma and Wisdom 1993, 1994; Laskar and Robutel 1993), or whether the changes ought to have been less intensive (Bills 2006; Paige et al. 2007). It has turned out that, for low initial inclinations, the orbit inclination reckoned from the precessing equator of date is subject only to small variations. This is an extension, to non-uniform equinoctial precession given by the Colombo model, of an old result obtained by Goldreich (1965) for the case of uniform precession and a low initial inclination. However, near-polar initial inclinations may exhibit considerable variations for up to ± 10 deg in magnitude. This result is accentuated when the obliquity is large. Nevertheless, the analysis confirms that an oblate planet can, indeed, afford large variations of the equinoctial precession over hundreds of millions of years, without repelling its near-equatorial satellites away from the equator of date: the satellite inclination oscillates but does not show a secular increase. Nor does it show secular decrease, a fact that is relevant to the discussion of the possibility of high-inclination capture of Phobos and Deimos.

Keywords Orbital elements · Osculating elements · Mars · Natural satellites · Natural satellites' orbits · Deimos · Equinoctial precession · The Goldreich lock

1 Introduction

1.1 Statement of purpose

The goal of this paper is to explore, by two very different methods, inclination variations of a solar-gravity-perturbed satellite orbiting an oblate planet subject to nonuniform equinoctial precession. This nonuniformity of precession is caused by the presence of the other planets. Their gravitational pull entails precession of the circumsolar orbit of our planet; this entails variations of the solar torque acting on it; these torque variations make the planet's equinoctial precession nonuniform; and this nonuniformity, in its turn, influences the behaviour of the planet's satellites. This influence is feeble, and we trace with a high accuracy whether it results, over aeons, in purely periodic changes in inclination or can accumulate to secular changes.

This work is but a small part of a larger project whose eventual goal is to build up a comprehensive tool for computation of long-term orbital evolution of satellites. Building this tool, block by block, we are beginning with only three components—the planet's oblateness, the direct pull of the Sun on the satellite, and the planet's precession. These phenomena bare a marked effect on the evolution of the orbit. In our subsequent publications, we shall incorporate more effects into our model—the triaxiality, and the bodily tides.

1.2 Motivation

One motivation for this work stems from our intention to carry out an independent check of whether the equinoctial-precession changes predicted for a rigid Mars by the Colombo model could have been sufficient to repel its moons away from the equator. An answer to this question, in combination with our knowledge of the current position of Phobos and Deimos, will help us to understand whether the Martian obliquity variations could indeed have undergone the large variations resulting from the Colombo model, or whether the actual variations ought to have smaller magnitude. Such a check is desirable because the current, Colombo-model-based theory of equinoctial precession (Ward 1973; Touma and Wisdom 1993, 1994;

Laskar and Robutel 1993), incorporates several approximations. First, the Colombo equation is derived under the assertion that the planet is rigid and is always in its principal spin state, the angular-momentum vector staying parallel to the angular-velocity one. Second, this description, being only a model, ignores the possibility of planetary catastrophes that might have altered the planet's spin mode. Third, this description ignores that sometimes even weak dissipation (caused, for example, by tides) may be sufficient to quell chaos and regularise the motion, which may be the case of Mars (Bills 2006). Fourth, it still remains a matter of controversy as to whether the observed pattern of small craters on Mars confirms (Hartmann 2007) or disproves (Paige et al. 2007) the strong climatic variations predicted in Ward (1974, 1979). All this motivates us to come up with a test based on the necessity to reconcile the variations of spin with the present near-equatorial positions of Phobos and Deimos. The fact that both moons found themselves on near-equatorial orbits, in all likelihood, billions of years ago,[1] and that both are currently located within less than 2 degrees from the equator, is surely more than a mere coincidence. An elegant but sketchy calculation by Goldreich (1965) demonstrated that the orbits of initially near-equatorial satellites remain close to the equator of date for as long as some simplifying assumptions remain valid. As explained in Efroimsky (2004, 2005), these assumptions are valid over time scales not exceeding 100 million years, while at longer times a more careful analysis is required. Its goal will be to explore the limits for the possible secular drift of the satellite orbits away from the evolving equator of date. Through comparison of these limits with the present location of the Martian satellites, we shall be able to impose restrictions upon the long-term spin variations of Mars. If, however, it turns out that near-equatorial satellites can, in the face of large equinoctial-precession variations, remain for billions of years close to the moving equator of date, then we shall admit that Mars' equator could indeed have precessed through billions of years in the manner predicted by the Colombo approximation.

The second motivation for our study comes from the ongoing discussion of whether the Martian satellites might have been captured at high inclinations, their orbits having gradually approached the equator afterwards. While a comprehensive check of this hypothesis will need a more detailed model—one that will include Mars' triaxiality, the tidal forces (Lainey et al. 2008), and perhaps other perturbations—the first, rough sketch of this test can be carried out with only J_2, the Sun, and the equinoctial precession taken into account. We perform such a rough check for a hypothetical satellite that has all the parameters of Deimos, except that its initial inclination is 89°.

[1] Phobos and Deimos give every appearance of being captured asteroids of the carbonaceous chondritic type, with cratered surfaces older than $\sim 10^9$ years (Veverka 1977; Pang et al. 1978; Pollack et al. 1979; Tolson et al. 1978). If they were captured by gas drag (Burns 1972, 1978), this must have occurred early in the history of the solar system while the gas disk was substantial enough. Kilgore, Burns, and Pollack (1978) have demonstrated numerically that a gas envelope extending to about ten Martian radii, with a density of 5×10^{-5} g/cm^3 at the Martian surface, could have been capable of capturing satellites of radii about 10 km. At that stage of planetary formation, the spin of the forming planet would be perpendicular to the planet's orbit about the Sun—i.e., the obliquity would be small and the gas disk would be nearly coplanar with the planetary orbit. Energetically, a capture would likely be equatorial. This is most easily seen in the context of the restricted three-body problem. The surfaces of zero velocity constrain any reasonable capture to occur from directions near the inner and outer collinear Lagrange points (Szebehely 1967; Murison 1988), which lie in the equatorial plane. Also, a somewhat inclined capture would quickly be equatorialised by the gas disk. If the capture inclination is too high, the orbital energy is then too high to allow a long enough temporary capture, and the object would hence not encounter enough drag over a long enough time to effect a permanent capture (Murison 1988). Thus, Phobos and Deimos were likely (in as much as we can even use that term) to have been captured into near-equatorial orbits.

1.3 Mathematical tools

The first steps toward the analytical theory of orbits about a precessing and nutating Earth were undertaken almost half a century ago by Brouwer (1959), Proskurin and Batrakov (1960), and Kozai (1960). The problem was considered, in application to the Martian satellites, by Goldreich (1965) and, in regard to a circumlunar orbiter, by Brumberg et al. (1971). The latter two publications addressed the dynamics as seen in a non-inertial frame co-precessing with the planet's equator of date. The analysis was carried out in terms of the so-called "contact" Kepler elements, i.e., in terms of the Kepler elements satisfying a condition different from that of osculation. Modeling of perturbed trajectories by sequences of instantaneous ellipses (or hyperbolae) parameterised with such elements is sometimes very convenient mathematically (Efroimsky 2006c). However, the physical interpretation of such solutions is problematic, because instantaneous conics defined by nonosculating elements are non-tangent to the trajectory. Though over restricted time scales the secular parts of the contact elements may well approximate the secular parts of their osculating counterparts (Efroimsky 2004, 2005), the cleavage between them may grow at longer time scales. This is the reason why a practically applicable treatment of the problem must be performed in the language of osculating variables.

1.4 The plan

The analytical theory of orbits about a precessing oblate primary, in terms of the Kepler elements defined in a co-precessing (i.e., related to the equator of date) frame, was formulated in Efroimsky (2006a, b) where the planetary equations were approximated by neglecting some high-order terms and averaging the others. This way, from the exact equations for osculating elements, approximate equations for their secular parts were obtained. We shall borrow those averaged Lagrange-type planetary equations, shall incorporate into them the pull of the Sun, and shall numerically explore their solutions. This will give us a method that will be semi-analytical and seminumerical. We shall then apply it to a particular setting—evolution of a Martian satellite and its reaction to the long-term variations of the spin state of Mars. Our goal will be to explore whether the spin-axis variations predicted for a rigid Mars permit its satellites to remain close to the equator of date for hundreds of millions through billions of years. In case the answer to this question turns out to be negative, it will compel us to seek nonrigidity-caused restrictions upon the spin variations. Otherwise, the calculations of the rigid-Mars inclination variations will remain in force (and so will the subsequent calculations of Mars obliquity variations); this way, the theory of Ward (1973, 1974, 1979, 1982), Touma and Wisdom (1993, 1994), and Laskar and Robutel (1993) will get a model-independent confirmation.

2 Semianalytical treatment of the problem

To understand the evolution of a satellite orbit about a precessing planet, it is natural to model it with elements defined in a coordinate system associated with the equator of date, i.e., in a frame co-precessing (but not co-rotating) with the planet. A transition from an inertial frame to the co-precessing one is a perturbation that depends not only upon the instantaneous position but also upon the instantaneous velocity of the satellite. It has been demonstrated by Efroimsky and Goldreich (2004) that such perturbations enter the planetary equations in a nontrivial way: not only do they alter the disturbing function (which is the negative

Hamiltonian perturbation) but also they endow the equations with several extra terms that are not parts of the disturbing function. Some of these nontrivial terms are linear in the planet's precession rate $\boldsymbol{\mu}$, some are quadratic in it; the rest are linear in its time derivative $\dot{\boldsymbol{\mu}}$. The inertial-forces-caused addition to the disturbing function (i.e., to the negative Hamiltonian perturbation) consists of a term linear and a term quadratic in $\boldsymbol{\mu}$. (See formulae (53–54) in Efroimsky (2004, 2005) or formulae (1) and (6) in Efroimsky (2006a, b).) The essence of approximation elaborated in Ibid. was to neglect the quadratic terms and to substitute the terms linear in $\boldsymbol{\mu}$ and $\dot{\boldsymbol{\mu}}$ with their secular parts calculated with precision up to e^3, inclusively.

2.1 Equations for the secular parts of osculating elements defined in a co-precessing reference frame

We shall begin with five Lagrange-type planetary equations for the secular parts of the orbital elements defined in a frame co-precessing with the equator of date. These equations, derived in Efroimsky (2004, 2005), have the following form:

$$\frac{da}{dt} = -2\frac{\dot{\mu}_\perp}{n} a \left(1 - e^2\right)^{1/2}, \tag{1}$$

$$\frac{de}{dt} = \frac{5}{2}\frac{\dot{\mu}_\perp}{n} e \left(1 - e^2\right)^{1/2}, \tag{2}$$

$$\begin{aligned}\frac{d\omega}{dt} = {} & \frac{3}{2}\frac{n\, J_2}{\left(1-e^2\right)^2}\left(\frac{\rho_e}{a}\right)^2\left(\frac{5}{2}\cos^2 i - \frac{1}{2}\right) - \mu_\perp + \mu_n \cot i \\ & - \frac{\cos i}{na^2(1-e^2)^{1/2}\sin i}\left\langle \dot{\boldsymbol{\mu}}\left(-\mathbf{f}\times\frac{\partial \mathbf{f}}{\partial i}\right)\right\rangle,\end{aligned} \tag{3}$$

$$\begin{aligned}\frac{di}{dt} = {} & -\mu_1\cos\Omega - \mu_2\sin\Omega + \frac{\cos i}{na^2(1-e^2)^{1/2}\sin i}\left\langle \dot{\boldsymbol{\mu}}\left(-\mathbf{f}\times\frac{\partial \mathbf{f}}{\partial \omega}\right)\right\rangle \\ & - \frac{1}{na^2\,(1-e^2)^{1/2}\sin i}\left\langle \dot{\boldsymbol{\mu}}\left(-\mathbf{f}\times\frac{\partial \mathbf{f}}{\partial \Omega}\right)\right\rangle,\end{aligned} \tag{4}$$

$$\begin{aligned}\frac{d\Omega}{dt} = {} & -\frac{3}{2} n\, J_2\left(\frac{\rho_e}{a}\right)^2 \frac{\cos i}{\left(1-e^2\right)^2} - \frac{\mu_n}{\sin i} \\ & + \frac{1}{n\, a^2(1-e^2)^{1/2}\sin i}\left\langle \dot{\boldsymbol{\mu}}\left(-\mathbf{f}\times\frac{\partial \mathbf{f}}{\partial i}\right)\right\rangle,\end{aligned} \tag{5}$$

The number of equations is five, because one element, M_o, was excluded by averaging of the Hamiltonian perturbation and of the inertial terms emerging in the right-hand sides. In the equations, $n \equiv \sqrt{G\left(m_{primary} + m_{secondary}\right)/a^3}$, while $\mathbf{f}(t; a, e, i, \omega, \Omega, M_o)$ is the implicit function that expresses the unperturbed two-body dependence of the position upon the time and Keplerian elements. Vector $\boldsymbol{\mu}$ denotes the total precession rate of the planetary equator (including all spin variations—from the polar wander and nutations through the Chandler wobble through the equinoctial precession through the longest-scale spin variations caused by the other planets' pull), while μ_1, μ_2, μ_3 stand for the components of $\boldsymbol{\mu}$ in

a co-precessing coordinate system x, y, z, the axes x and y belonging to the equator-of-date plane, and the longitude of the node, Ω, being reckoned from x:

$$\boldsymbol{\mu} = \mu_1 \hat{\mathbf{x}} + \mu_2 \hat{\mathbf{y}} + \mu_3 \hat{\mathbf{z}}, \qquad \text{where} \quad \mu_1 = \dot{I}_p, \quad \mu_2 = \dot{h}_p \sin I_p, \quad \mu_3 = \dot{h}_p \cos I_p, \tag{6}$$

I_p, h_p being the inclination and the longitude of the node of the equator of date relative to that of epoch, and a dot standing for a time derivative. The quantity $\mu_\perp$ is a component of $\boldsymbol{\mu}$ directed along the instantaneous orbital momentum of the satellite, i.e., perpendicular to the instantaneous osculating Keplerian ellipse. This component is expressed with

$$\mu_\perp \equiv \boldsymbol{\mu} \cdot \mathbf{w} = \mu_1 \sin i \sin \Omega - \mu_2 \sin i \cos \Omega + \mu_3 \cos i, \tag{7}$$

the unit vector

$$\mathbf{w} = \hat{\mathbf{x}} \sin i \sin \Omega - \hat{\mathbf{y}} \sin i \cos \Omega + \hat{\mathbf{z}} \cos i \tag{8}$$

standing for the unit normal to the instantaneous osculating ellipse. Be mindful that $\dot{\mu}_\perp$ is defined not as $d(\boldsymbol{\mu} \cdot \mathbf{w})/dt$ but as

$$\dot{\mu}_\perp \equiv \dot{\boldsymbol{\mu}} \cdot \mathbf{w} = \dot{\mu}_1 \sin i \sin \Omega - \dot{\mu}_2 \sin i \cos \Omega + \dot{\mu}_3 \cos i. \tag{9}$$

The quantity μ_n is a component pointing within the satellite's orbital plane, in a direction orthogonal to the line of nodes of the satellite orbit relative to the equator of date:

$$\begin{aligned} \mu_n &= -\mu_1 \sin \Omega \cos i + \mu_2 \cos \Omega \cos i + \mu_3 \sin i \\ &= -\dot{I}_p \sin \Omega \cos i + \dot{h}_p \sin I_p \cos \Omega \cos i + \dot{h}_p \cos I_p \sin i. \end{aligned} \tag{10}$$

Its time derivative taken in the frame of reference co-precessing with the equator of date is:

$$\begin{aligned} \dot{\mu}_n &= -\dot{\mu}_1 \sin \Omega \cos i + \dot{\mu}_2 \cos \Omega \cos i + \dot{\mu}_3 \sin i \\ &= -\ddot{I}_p \sin \Omega \cos i + \left(\ddot{h}_p \sin I_p + \dot{h}_p \dot{I}_p \cos I_p\right) \cos \Omega \cos i \\ &\quad + \left(\ddot{h}_p \cos I_p - \dot{h}_p \dot{I}_p \sin I_p\right) \sin i. \end{aligned} \tag{11}$$

As shown in Efroimsky (2006a, b), the $\dot{\boldsymbol{\mu}}$-dependent terms, emerging in Eqs. 1–5, are expressed with

$$\begin{aligned} \left\langle \dot{\boldsymbol{\mu}} \cdot \left(-\mathbf{f} \times \frac{\partial \mathbf{f}}{\partial i} \right) \right\rangle = \frac{a^2}{4} \Big\{ & \dot{\mu}_1 \left[-\left(2 + 3\, e^2\right) \cos \Omega + 5\, e^2 \left(\cos \Omega \cos 2\omega - \sin \Omega \sin 2\omega \cos i\right) \right] \\ & + \dot{\mu}_2 \left[-\left(2 + 3\, e^2\right) \sin \Omega + 5\, e^2 \left(\sin \Omega \cos 2\omega + \cos \Omega \sin 2\omega \cos i\right) \right] \\ & + \dot{\mu}_3 \left[5 e^2 \sin 2\omega \sin i \right] \Big\} \end{aligned} \tag{12}$$

$$\left\langle \dot{\boldsymbol{\mu}} \cdot \left(-\mathbf{f} \times \frac{\partial \mathbf{f}}{\partial \omega} \right) \right\rangle = -\frac{a^2}{2} \left(2 + 3e^2\right) \left(\dot{\mu}_1 \sin i \sin \Omega - \dot{\mu}_2 \sin i \cos \Omega + \dot{\mu}_3 \cos i\right), \tag{13}$$

$$\begin{aligned} \left\langle \dot{\boldsymbol{\mu}} \cdot \left(-\mathbf{f} \times \frac{\partial \mathbf{f}}{\partial \Omega} \right) \right\rangle = \frac{a^2}{4} \Big\{ & \dot{\mu}_1 \sin i \left[-\left(2 + 3\, e^2\right) \sin \Omega \cos i \right. \\ & \left. + 5 e^2 \left(\cos \Omega \sin 2\omega + \sin \Omega \cos 2\omega \cos i\right) \right] \\ & + \dot{\mu}_2 \sin i \left[\left(2 + 3\, e^2\right) \cos \Omega \cos i \right. \\ & \left. + 5\, e^2 \left(\sin \Omega \sin 2\omega - \cos \Omega \cos 2\omega \cos i\right) \right] \\ & - \dot{\mu}_3 \left[\left(2 + 3\, e^2\right) \left(2 - \sin^2 i\right) + 5\, e^2 \sin^2 i \cos 2\omega \right] \Big\} \end{aligned} \tag{14}$$

To integrate Eqs. 1–5, with expressions (12–14) inserted therein, we shall need to know, at each step of integration, the components of $\boldsymbol{\mu}$ and $\dot{\boldsymbol{\mu}}$.

2.2 Calculation of the components of μ and $\dot{\mu}$

At each step of our integration, the components of $\boldsymbol{\mu}$ and $\dot{\boldsymbol{\mu}}$ will be calculated in the Colombo approximation. Physically, the essence of this approximation is two-fold: first, the solar torque acting on the planet is replaced by its average over the year; and, second, the precessing planet is assumed to be always in its principal spin state. While a detailed development (based on the work by Colombo 1966) may be found in the Appendix to Efroimsky (2006a, b), here we shall provide a concise list of resulting formulae to be used.

The components of $\boldsymbol{\mu}$ are connected, through the medium of (6), with the inclination and the longitude of the node of the moving planetary equator, I_p and h_p, relative to some equator of epoch. These quantities and their time derivatives are connected with the unit vector $\hat{\mathbf{k}}$ aimed in the direction of the major-inertia axis of the planet:

$$\hat{\mathbf{k}} = \left(\sin I_p \, \sin h_p, \quad -\sin I_p \, \cos h_p, \quad \cos I_p\right)^T. \tag{15}$$

This unit vector and its time derivative

$$\begin{aligned} \frac{d\hat{\mathbf{k}}}{dt} = \big(&\dot{I}_p \cos I_p \sin h_p + \dot{h}_p \sin I_p \cos h_p, \\ &-\dot{I}_p \cos I_p \cos h_p + \dot{h}_p \sin I_p \sin h_p, \quad -\dot{I}_p \sin I_p\big)^T, \end{aligned} \tag{16}$$

depend, through the Colombo equation

$$\frac{d\hat{\mathbf{k}}}{dt} = \alpha \left(\hat{\mathbf{n}} \cdot \hat{\mathbf{k}}\right) \left(\hat{\mathbf{k}} \times \hat{\mathbf{n}}\right), \tag{17}$$

upon the unit normal to the planetary orbit,

$$\hat{\mathbf{n}} = \left(\sin I_{orb} \sin \Omega_{orb}, \quad -\sin I_{orb} \cos \Omega_{orb}, \quad \cos I_{orb}\right)^T, \tag{18}$$

Ω_{orb} and I_{orb} being the node and inclination of the orbit relative to some fiducial fixed plane, and α being a parameter proportional to the oblateness factor J_2. In our computations, we employed the present-day[2] value of α—see Table 5 below. We chose this value because it was the one used by Ward (1973, 1974), and we wanted to make sure that our plot for obliquity evolution, Fig. 3, coincided with that of Ward (1974).

To find the components of $\boldsymbol{\mu}$, one must know the time evolution of h_p and I_p, which can be determined by solving a system of three differential equations (17), with Ω_{orb} and I_{orb} being some known functions of time. These functions may be computed via the auxiliary variables

$$q = \sin I_{orb} \sin \Omega_{orb}, \quad p = \sin I_{orb} \cos \Omega_{orb}, \tag{19}$$

[2] An accurate treatment shows that due to the precession of the Martian orbit α exhibits quasi-periodic variations of about 3% over long time scales. Neglecting this detail in the current work, we shall take it into account at the further stage of our project (Lainey et al. 2008).

Table 1 Numerical values used in Ward's model of the inclination and node of the Martian orbit

j	N_j	s'_j [arcsec/yr]	δ'_j [deg]
1	0.0018011	−5.201537	272.06
2	0.0018012	−6.570802	210.06
3	−0.0358910	−18.743586	147.39
4	0.0502516	−17.633305	188.92
5	0.0096481	−25.733549	19.58
6	−0.0012561	−2.902663	207.48
7	−0.0012286	−0.677522	95.01

whose evolution will be given by the formulae:

$$q = \sum_{j=1}^{\infty} N_j \sin\left(s'_j t + \delta_j\right), \tag{20}$$

$$p = \sum_{j=1}^{\infty} N_j \cos\left(s'_j t + \delta_j\right). \tag{21}$$

The choice of amplitudes, frequencies, and phases as in Table 1 will make equations (19–21) render Ω_{orb} and I_{orb} relative to the solar system's invariable plane (Ward 1974).[3]

The development by Ward (1974) is limited in precision. A more accurate treatment was offered by Laskar (1988). At the future stages of our project, when developing a detailed physical model of the satellite motion, we shall employ Laskar's results. In the current paper, we are checking if the orbital averaging of the precession-caused terms is permissible at large time scales. Hence, for the purpose of this check, as well for the qualitative estimate of the long-term behaviour of the satellites, we need a realistic, not necessarily highly accurate, scenario of the precession variations.

2.3 The Goldreich approximation

The above semianalytical treatment not only yields plots of the time dependence of the mean elements but also serves as a launching pad for analytical approximations. For example, an assumption of a and e being constant, and a neglect of the $\dot{\boldsymbol{\mu}}$-dependent terms in (4–5), as well as of the term $\mu_n / \sin i$ in (5), gives birth to the Goldreich (1965) approximation:

$$\frac{da}{dt} = 0, \tag{22}$$

$$\frac{de}{dt} = 0, \tag{23}$$

$$\frac{di}{dt} = -\mu_1 \cos\Omega - \mu_2 \sin\Omega, \tag{24}$$

[3] Ward (1974) has calculated the values of the coefficients N, s', δ based on the work of Brouwer and van Woerkom (1950) who had calculated the values of p and q relative to the ecliptic plane of 1950. Ward (1974) transformed Brouwer and van Woerkom's values to the solar system's invariable plane. Be mindful that, no matter what the reference plane, both Ward (1974) and Brouwer and van Woerkom (1950) used the same epoch, J1950.

$$\frac{d\Omega}{dt} = -\frac{3}{2} n J_2 \left(\frac{\rho_e}{a}\right)^2 \frac{\cos i}{(1-e^2)^2}, \tag{25}$$

$$\frac{d\omega}{dt} = \frac{3}{4} n\ J_2 \left(\frac{\rho_e}{a}\right)^2 \frac{5\cos^2 i - 1}{(1-e^2)^2} + \frac{\mu_n \cos i}{\sin i} - \mu_\perp, \tag{26}$$

the equinoctial precession being assumed uniform:

$$\dot{I}_p = 0 \tag{27}$$

$$\dot{h}_p = -\alpha \cos I_p \tag{28}$$

$$\mu_1 = 0 \tag{29}$$

$$\mu_2 = \dot{h}_p \sin I_p \tag{30}$$

$$\mu_3 = \dot{h}_p \cos I_p. \tag{31}$$

For the details of Goldreich's approximation see also Subsect. 3.3 in Efroimsky (2005).

2.4 The gravitational pull of the Sun

Reaction of a satellite on the planetary-equator precession is, in a way, an indirect reaction of the satellite on the presence of the Sun and the other planets. Indeed, the pull of the other planets makes the orbit of our planet precess, which entails variations in the Sun-produced gravitational torque acting on the planet. These variations of the torque, in their turn, lead to the variable equinoctial precession of the equator, precession "felt" by the satellite. It would be unphysical to consider this, indirect effect of the Sun and the planets upon the satellite, without taking into account their direct gravitational pull. In this subsection, we shall take into account the pull of the Sun, which greatly dominates that of the planets other than the primary.

In what follows, m and m' will be the masses of the satellite and the Sun, correspondingly, $\mathbf{r}$ and $\mathbf{r}'$ will stand for the planetocentric positions of the satellite and the Sun, S will signify the angle between these vectors. Then the Sun-caused perturbing potential R_S, acting on the satellite, will assume the form of

$$R_S = Gm' \left(\frac{1}{|\mathbf{r}' - \mathbf{r}|} - \frac{\mathbf{r}' \cdot \mathbf{r}}{r'^3}\right) = \frac{Gm'}{r'} \left(\frac{r'}{|\mathbf{r}' - \mathbf{r}|} - \frac{r\cos S}{r'}\right) \tag{32}$$

This can be expanded in a usual manner over the Legendre polynomials of the first kind. Since $r' \gg r$, we shall take only the first term in the series:[4]

$$R_S \approx \frac{Gm'}{r'} \left[1 + \frac{r}{r'} P_1(\cos S) + \left(\frac{r}{r'}\right)^2 P_2(\cos S) - \frac{r\cos S}{r'}\right] \tag{33}$$

As the term Gm'/r' is not dependent of the satellite's elements, one has only to consider the restricted potential

$$R_S^1 = \frac{Gm'}{r'} \left[\left(\frac{r}{r'}\right)^2 P_2(\cos S)\right] \approx \frac{n'^2 a^2}{2} \left(\frac{a'}{r'}\right)^3 (3\cos^2 S - 1), \tag{34}$$

n' and a' being the mean motion and the semi-major axis of the Sun.

To obtain the Lagrange-type equations for the third-body perturbation, we must first derive an expression for the angle S. To that end, define the directional cosines $\xi \equiv \hat{\mathbf{P}} \cdot \hat{\mathbf{r}}'$ and

[4] This is justified since the next term in the Legendre series is about 2 orders of magnitude smaller than the potential variations generated by the precession.

$\theta \equiv \hat{\mathbf{Q}} \cdot \hat{\mathbf{r}}'$, where $\hat{\mathbf{r}}'$ is a unit vector pointing from the planet toward the Sun, while $\hat{\mathbf{P}}$ and $\hat{\mathbf{Q}}$ are unit vectors of a perifocal coordinate system associated with the osculating orbital plane of the satellite, with $\hat{\mathbf{P}}$ pointing to the instantaneous periapse and $\hat{\mathbf{Q}}$ being orthogonal to $\hat{\mathbf{P}}$. Assuming that the planet's orbit about the Sun is circular, we arrive at

$$\xi = \cos\omega\cos(\Omega - M') - \cos i \sin\omega \sin(\Omega - M'), \tag{35}$$

$$\theta = -\sin\omega\cos(\Omega - M') - \cos i \cos\omega \sin(\Omega - M'), \tag{36}$$

where M' is the mean anomaly of the Sun in the planetocentric frame. With aid of these relations, the angle S may be written down as

$$\cos S = \xi \cos\nu + \theta \sin\nu, \tag{37}$$

ν being the true anomaly of the satellite in the planetocentric coordinate system. Substituting (35) and (36) into (37), and averaging over the satellite's mean anomaly, we arrive at the Lagrange-type equations:

$$\frac{da}{d\tau} = 0 \tag{38a}$$

$$\frac{de}{d\tau} = 10\, e\sqrt{1-e^2}\left[\sin^2 i \sin 2\omega + (2 - \sin^2 i)\sin 2\omega \cos 2\tilde{\Omega} + 2\cos i \cos 2\omega \sin 2\tilde{\Omega}\right] \tag{38b}$$

$$\frac{di}{d\tau} = -\frac{2\sin i}{\sqrt{1-e^2}}\left\{5e^2 \cos i \sin 2\omega(1 - \cos 2\tilde{\Omega}) - \left[2 + e^2(3 + 5\cos 2\omega)\right]\sin 2\tilde{\Omega}\right\} \tag{38c}$$

$$\frac{d\omega}{d\tau} = \frac{2}{\sqrt{1-e^2}}\left\{4 + e^2 - 5\sin^2 i + 5(\sin^2 i - e^2)\cos 2\omega + 5(e^2 - 2) \times \cos i \sin 2\omega \sin 2\tilde{\Omega} + \left[5(2 - e^2 - \sin^2 i)\cos 2\omega - 2 - 3\,e^2 + 5\sin^2 i\right] \times \cos 2\tilde{\Omega}\right\} \tag{38d}$$

$$\frac{d\tilde{\Omega}}{d\tau} = -\kappa - \frac{2}{\sqrt{1-e^2}}\left\{\left[2 + e^2(3 - 5\cos 2\omega)\right](1 - \cos 2\tilde{\Omega})\cos i - 5e^2 \sin 2\omega \sin 2\tilde{\Omega}\right\} \tag{38e}$$

where we used the following set of notations:

$$\tau \equiv \beta n(t - t_0), \quad \beta = \frac{3\, m' a^3}{16\, M\, a'^3} \tag{39}$$

$$\kappa \equiv \frac{16\, n}{3\, n'}\left(1 + \frac{M}{m'}\right) \tag{40}$$

$$\tilde{\Omega} \equiv \Omega - \lambda', \tag{41}$$

λ' being the mean longitude of the Sun in the planet's frame, and M being the mass of Mars.

An additional averaging can be performed over the motion of the planet about the Sun. Mathematically, this is the same as averaging over the motion of the Sun about the planet—in both cases averaging over λ' is implied. This averaging (Innanen et al. 1997) will simplify (38) into

$$\frac{da}{dt} = 0 \tag{42a}$$

$$\frac{de}{dt} = 10e\sqrt{1-e^2}\beta n \sin^2 i \sin 2\omega \tag{42b}$$

$$\frac{di}{dt} = -\frac{10e^2 \sin i}{\sqrt{1-e^2}}\beta n \cos i \sin 2\omega \tag{42c}$$

$$\frac{d\omega}{dt} = \frac{2}{\sqrt{1-e^2}}\beta n \left[4 + e^2 - 5\sin^2 i + 5(\sin^2 i - e^2)\cos 2\omega\right] \tag{42d}$$

$$\frac{d\Omega}{dt} = -\frac{2}{\sqrt{1-e^2}}\beta n \left[2 + e^2(3 - 5\cos 2\omega)\right]\cos i \tag{42e}$$

It is important to note that the calculations leading to equations (38), and to their double-averaged version, (42), were performed in the Martian-orbital, and not Martian-equatorial frame, without taking either the Martian obliquity or precession into consideration. Had we taken into account the precession, we would get, on the right-hand side of (42) resonances between the motion of the Sun relative to the planet and the equinoctial precession. Since the time scale of the former exceeds, by orders of magnitude, the time scale of the latter, we may safely omit such resonances. This justifies our neglect of the frame precession in the above calculation.

However, the omission of the obliquity may have a serious effect on the results. Thus, we shall generalize equations (38) so as to include the effect of the solar inclination and node in a Martian-centric frame. This generalized model based on the celebrated works by Kozai (1959) and Cook (1962) gives us:

$$\frac{da}{dt} = 0 \tag{43a}$$

$$\frac{de}{dt} = -\frac{15n'^2 e\sqrt{1-e^2}}{4n}\left[2AB\cos(2\omega) - (A^2 - B^2)\sin(2\omega)\right] \tag{43b}$$

$$\frac{di}{dt} = \frac{3n'^2 C}{4n\sqrt{1-e^2}}\left\{A\left[2 + 3e^2 + 5e^2\cos(2\omega)\right] + 5Be^2\sin(2\omega)\right\} \tag{43c}$$

$$\begin{aligned}\frac{d\omega}{dt} = &-\dot{\Omega}\cos i + \frac{3n'^2\sqrt{1-e^2}}{2n} \\ &\times\left[5AB\sin(2\omega) + \frac{5}{2}(A^2 - B^2)\cos(2\omega) - 1 + \frac{3(A^2+B^2)}{2}\right] \\ &+\frac{15n'^2 a(A\cos\omega + B\sin\omega)}{4nea'}\left[1 - \frac{5}{4}(A^2 + B^2)\right]\end{aligned} \tag{43d}$$

$$\frac{d\Omega}{dt} = \frac{3n'^2 C}{4n\sqrt{1-e^2}\sin i}\left\{5Ae^2\sin(2\omega) + B\left[2 + 3e^2 - 5e^2\cos(2\omega)\right]\right\} \tag{43e}$$

where

$$A = \cos(\Omega - \Omega')\cos(\lambda') + \cos(i')\sin(\lambda')\sin(\Omega - \Omega') \tag{44a}$$

$$B = \cos i\left[-\sin(\Omega - \Omega')\cos(\lambda') + \cos(i')\sin(\lambda')\cos(\Omega - \Omega')\right] + \sin i\sin(i')\sin(\lambda') \tag{44b}$$

$$C = \sin i\left[\cos\lambda'\sin(\Omega - \Omega') - \cos(i')\sin(\lambda')\cos(\Omega - \Omega')\right] + \cos i\sin i'\sin\lambda' \tag{44c}$$

Here, i' and Ω' are the inclination and right ascension of the ascending node of the Solar orbit in the Martian equatorial frame, respectively. The doubly averaged equations, obtained after averaging over the Sun's mean anomaly for a single period, are given by

$$\frac{da}{dt} = 0 \tag{45a}$$

$$\frac{de}{dt} = -\frac{15n'^2 e\sqrt{1-e^2}}{4n}\left[2\overline{AB}\cos(2\omega) - (\overline{A^2} - \overline{B^2})\sin(2\omega)\right] \tag{45b}$$

$$\frac{di}{dt} = \frac{3n'^2}{4n\sqrt{1-e^2}}\left\{\overline{CA}\left[2 + 3e^2 + 5e^2\cos(2\omega)\right] + 5\overline{CB}e^2\sin(2\omega)\right\} \tag{45c}$$

$$\frac{d\omega}{dt} = -\dot{\Omega}\cos i + \frac{3n'^2\sqrt{1-e^2}}{2n} \times\left[5\overline{AB}\sin(2\omega) + \frac{5}{2}(\overline{A^2} - \overline{B^2})\cos(2\omega) - 1 + \frac{3(\overline{A^2} + \overline{B^2})}{2}\right] \tag{45d}$$

$$\frac{d\Omega}{dt} = \frac{3n'^2}{4n\sqrt{1-e^2}\sin i}\left\{5\overline{CA}e^2\sin(2\omega) + \overline{CB}\left[2 + 3e^2 - 5e^2\cos(2\omega)\right]\right\} \tag{45e}$$

the averaged quantities $\overline{A^2}$, $\overline{B^2}$, $\overline{AB}$, $\overline{AC}$, $\overline{BC}$ being given by

$$\overline{A^2} = \left[\mathrm{s}_{i'}^2\mathrm{c}_{\Omega'}^2 - 0.5\,\mathrm{s}_{i'}^2\right]\mathrm{c}_\Omega^2 + \mathrm{s}_{i'}^2\mathrm{s}_{\Omega'}\mathrm{s}_{\Omega'}\mathrm{s}_\Omega\mathrm{c}_{\Omega'}\mathrm{c}_\Omega + 0.5 - 0.5\mathrm{s}_{i'}^2\mathrm{c}_{\Omega'}^2 \tag{46a}$$

$$\overline{B^2} = \left\{\left(\mathrm{s}_{i'}^2\mathrm{c}_{\Omega'}^2 + 0.5\mathrm{s}_{i'}^2\right)\mathrm{c}_\Omega^2 - \mathrm{s}_{\Omega'}\mathrm{s}_{i'}^2\mathrm{s}_\Omega\mathrm{c}_{\Omega'}\mathrm{c}_\Omega + 0.5\mathrm{s}_{i'}^2\mathrm{c}_{\Omega'}^2 - 0.5 + \mathrm{c}_{i'}^2\right\}\mathrm{c}_i^2 + \left(\mathrm{c}_{i'}\mathrm{c}_\Omega\mathrm{c}_{\Omega'} + \mathrm{c}_{i'}\mathrm{s}_\Omega\mathrm{s}_{\Omega'}\right)\mathrm{s}_{i'}\mathrm{s}_i\mathrm{c}_i + 0.5\mathrm{s}_{i'}^2 \tag{46b}$$

$$\overline{AB} = \left\{\mathrm{s}_{i'}^2\mathrm{s}_{\Omega'}\mathrm{c}_{\Omega'}\mathrm{c}_\Omega^2 + \left[-\mathrm{s}_{i'}^2\mathrm{s}_\Omega\mathrm{c}_{\Omega'}^2 + 0.5\mathrm{s}_{i'}^2\mathrm{s}_\Omega\right]\mathrm{c}_\Omega - 0.5\mathrm{s}_{i'}^2\mathrm{s}_{\Omega'}\mathrm{c}_{\Omega'}\right\}\mathrm{c}_i + 0.5\mathrm{c}_{i'}\left(\mathrm{s}_\Omega\mathrm{c}_{\Omega'} - \mathrm{c}_\Omega\mathrm{s}_{\Omega'}\right)\mathrm{s}_{i'}\mathrm{s}_i \tag{46c}$$

$$\overline{AC} = 0.5\,\mathrm{c}_{i'}\left(\mathrm{s}_\Omega\mathrm{c}_{\Omega'} - \mathrm{c}_\Omega\mathrm{s}_{\Omega'}\right)\mathrm{s}_{i'}\mathrm{c}_i + \left\{-\mathrm{s}_{i'}^2\mathrm{s}_{\Omega'}\mathrm{c}_{\Omega'}\mathrm{c}_\Omega^2 + \left[-\mathrm{s}_{i'}^2((\mathrm{s}_\Omega)^2\mathrm{c}_{\Omega'}^2)\right]\mathrm{c}_\Omega + 0.5\mathrm{s}_{i'}^2\mathrm{s}_{\Omega'}\mathrm{c}_{\Omega'}\right\}\mathrm{s}_i \tag{46d}$$

$$\overline{BC} = \left(\mathrm{c}_{i'}\mathrm{c}_\Omega\mathrm{c}_{\Omega'} + \mathrm{c}_{i'}\mathrm{s}_\Omega\mathrm{s}_{\Omega'}\right)\mathrm{s}_{i'}\mathrm{c}_i^2 + \left\{\left[\mathrm{s}_{i'}^2\left(\mathrm{c}_{\Omega'}\right)^2 - 0.5\left(s_{i'}\right)^2\right]\mathrm{c}_\Omega^2 - \mathrm{s}_{i'}^2\mathrm{s}_{\Omega'}\mathrm{s}_\Omega\mathrm{c}_{\Omega'}\mathrm{c}_\Omega + -0.5\mathrm{s}_{i'}^2\mathrm{c}_{\Omega'}^2 - \mathrm{c}_{i'}^2 + 0.5\right\}\mathrm{s}_i\mathrm{c}_i - 0.5\left(\mathrm{c}_{i'}\mathrm{s}_\Omega\mathrm{s}_{\Omega'} + \mathrm{c}_{i'}\mathrm{c}_\Omega\mathrm{c}_{\Omega'}\right)\mathrm{s}_{i'} \tag{46e}$$

where we have used the compact notation $\mathrm{c}_{(\cdot)} = \cos(\cdot)$, $\mathrm{s}_{(\cdot)} = \sin(\cdot)$. To calculate the trigonometric functions of Ω' and i' appearing in equations (46), we shall utilise the geometry rendered Fig. 1. The figure depicts the Martian spin axis, $\hat{\mathbf{k}}$, that is perpendicular to the equator of date, and the normal to the orbital plane (ecliptic of date), $\hat{\mathbf{n}}$. The Martian obliquity, ϵ, is the angle between these two vectors, and is calculated based on the Colombo formalism:

$$\cos\epsilon = \hat{\mathbf{k}}\cdot\hat{\mathbf{n}} = q\,s_x + p\,s_y + F\,s_z \tag{47}$$

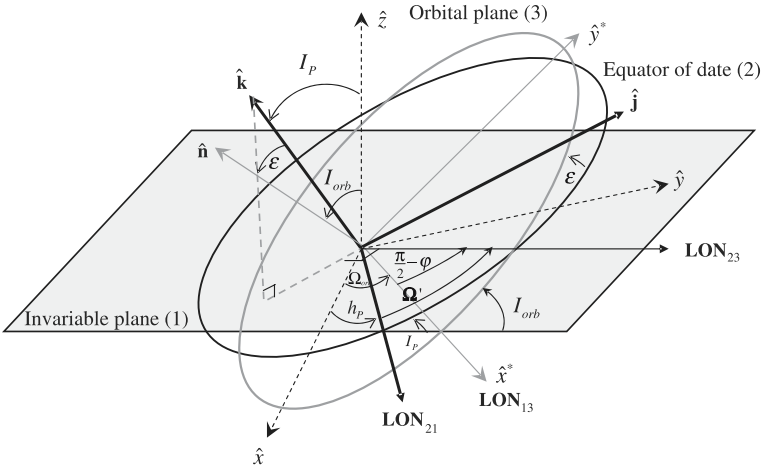

Fig. 1 The geometry of the precessing Mars. The Martian spin axis, $\hat{\mathbf{k}}$, is perpendicular to the equator of date, and the normal to the orbital plane (ecliptic of date), $\hat{\mathbf{n}}$. The Martian obliquity, ϵ, is the angle between these two vectors

where

$$s_x = \sin I_p \sin h_p, \quad s_y = \sin I_p \cos h_p, \quad s_z = \cos I_p, \quad F = \sqrt{1 - p^2 - q^2} \tag{48}$$

and $i' = \epsilon$.

The angle Ω', lying in the equator of date, is subtended between the vectors $\mathbf{LON}_{12}$ and $\mathbf{LON}_{23}$. The first of these, $\mathbf{LON}_{12}$, points along the line-of-nodes obtained by the intersection of the equator of date and the invariable plane. This vector must be perpendicular to the plane defined by $\hat{\mathbf{k}}$ and $\hat{\mathbf{z}}$ (the normal to the invariable plane), so that

$$\mathbf{LON}_{21} = \hat{\mathbf{z}} \times \hat{\mathbf{k}} = [s_y, s_x, 0]^T \tag{49}$$

The second vector, $\mathbf{LON}_{23}$, is aimed along the line of nodes rendered by the intersection of the orbital plane and the equator of date. Based on the geometry of Fig. 1, we write:

$$\mathbf{LON}_{23} = \hat{\mathbf{k}} \times \hat{\mathbf{n}} = [-s_y F + s_z\, p, \quad s_z q - s_x F, \quad -s_x p + s_y q]^T \tag{50}$$

By taking the scalar product of $\mathbf{LON}_{23}$ and $\mathbf{LON}_{21}$, we derive the direction cosine:

$$\cos \Omega' = \frac{\mathbf{LON}_{23} \cdot \mathbf{LON}_{21}}{|\mathbf{LON}_{23}||\mathbf{LON}_{21}|} = \frac{\cos I_p \cos i' - \cos I_{orb}}{\sin I_p \sin i'} \tag{51}$$

To derive an expression for $\sin \Omega'$, we shall have to compute an auxiliary vector, $\hat{\mathbf{j}}$, which lies in the orbital plane and is normal to both $\hat{\mathbf{k}}$ and $\mathbf{LON}_{21}$ (cf. Fig. 1):

$$\hat{\mathbf{j}} \equiv \hat{\mathbf{k}} \times \mathbf{LON}_{21} = [-s_z s_x, \quad s_z s_y, \quad s_x^2 + s_y^2]^T \tag{52}$$

The direction cosine between $\hat{\mathbf{j}}$ and $\mathbf{LON}_{23}$ is then

$$\cos\left(\frac{\pi}{2} - \Omega'\right) = \frac{\mathbf{LON}_{23} \cdot \hat{\mathbf{j}}}{|\mathbf{LON}_{23}||\hat{\mathbf{j}}|} \tag{53}$$

Upon evaluating Eq. 53 we arrive at

$$\sin\Omega' = \frac{q\cos h_p - p\sin h_p}{\sin i'} \tag{54}$$

Finally, the calculation of the orbital-elements' evolution is performed via Lagrange-type planetary equations, whose right-hand sides combine those of (1)–(5) and (45).

2.5 The higher-order harmonics, the gravitational pull of the planets, the Yarkovsky effect, and the bodily tides

In the current paper, we pursue a limited goal of taking into account the oblateness of the planet, its nonuniform equinoctial precession, and the gravitational pull of the Sun. These three items certainly do not exhaust the list of factors influencing the orbit evolution of a satellite.

Among the factors that we intend to include into the model at the further stage of its development are the high-order zonal (J_3, J_4, J_2^2) and tesseral (C_{22}) harmonics of the planet's gravity field, as well as the gravitational pull of the other planets—factors whose role was comprehensively discussed, for example, by Waz (2004). We also intend to include the bodily tides (Efroimsky and Lainey 2007) and the Yarkovsky effect (Nesvorný and Vokrouhlický 2007)—factors whose importance increases at long time scales.

3 Comparison of a purely numerical and a semianalytical treatment of the problem

One of our goals is to check the applicability limits (both in terms of the initial conditions and the permissible time scales) of our semianalytical model written for the osculating elements introduced in a frame co-precessing with the equator of date. This check will be performed by an independent, purely numerical, computation that will be free from whatever simplifying assumptions (all terms kept, no averaging performed.) The straightforward simulation will be carried out in terms of Cartesian coordinates and velocities defined in an inertial frame of reference. Both the semianalytical calculation of the elements in a co-precessing frame and the straightforward numerical integration in inertial Cartesian axes will be carried out for Deimos.

3.1 Integration by a purely numerical approach

The numerical integration of Deimos' orbit can be performed using Cartesian coordinates defined relatively to the Solar system invariable plane. As we also have to compute the Martian polar axis motion, there are two vector differential equations to integrate simultaneously. One is the Newton gravity law:

$$\ddot{\mathbf{r}} = -\frac{G(M+m)\mathbf{r}}{r^3} + Gm'\left(\frac{\mathbf{r}'-\mathbf{r}}{|\mathbf{r}'-\mathbf{r}|^3} - \frac{\mathbf{r}'}{r'^3}\right) + G(M+m)\nabla U, \tag{55}$$

where ∇U has components

$$\begin{cases} \partial_x U = \dfrac{\rho_e^2 J_2}{r^4}\left[\dfrac{x}{r}\left(\dfrac{15}{2}\sin^2\phi - \dfrac{3}{2}\right) - 3\sin\phi\sin I_p\sin h_p\right] \\ \partial_y U = \dfrac{\rho_e^2 J_2}{r^4}\left[\dfrac{y}{r}\left(\dfrac{15}{2}\sin^2\phi - \dfrac{3}{2}\right) + 3\sin\phi\sin I_p\cos h_p\right] \\ \partial_z U = \dfrac{\rho_e^2 J_2}{r^4}\left[\dfrac{z}{r}\left(\dfrac{15}{2}\sin^2\phi - \dfrac{3}{2}\right) - 3\sin\phi\cos I_p\right]. \end{cases} \tag{56}$$

Here ϕ and $\mathbf{r} = (x, y, z)$ denote, correspondingly, the latitude of Deimos relative to the Martian equator and the position vector of Deimos related to the Martian center of mass; ρ_e is the Martian equatorial radius; M and m stand for the masses of Mars and Deimos, respectively. Angles h_p and I_p are the longitude of the node and the inclination of the planet's equator of date relative to the invariable plane (see Sect. 2.2). Integration in this, inertial, frame offers the obvious advantage of nullifying the inertial forces.

Table 2 gives the initial conditions for our simulation, expressed in terms of the Keplerian orbital elements. Table 3 presents these initial conditions in a more practical form, i.e., in terms of the Cartesian positions and velocities corresponding to the said elements. A transition from the Keplerian elements to these Cartesian positions and velocities is a two-step process. First, we take orbital elements defined in a frame associated with the Martian equator of date (i.e., in a frame co-precessing but not co-rotating with the planet) and transform them into Cartesian coordinates and velocities defined in that same frame. Then, by two successive rotations of angles $-I_p$ and $-h_p$, we transform them into Cartesian coordinates and velocities related to the invariable plane. These initial positions and velocities were used to begin the integration.

At each step of integration of (55), the same two rotations are performed on the components ∇U given by (56). As mentioned above, to afford the absence of inertial forces on the right-hand side of (55) one must write down and integrate (55) in the inertial frame. Since the analytical expressions (56) for ∇U contain the latitude ϕ, they are valid in the co-precessing coordinate system and, therefore, need to be transformed to the inertial frame at each step. To carry out the transformation, one needs to know, at each step, the relative orientation of the Martian polar axis and the inertial coordinate system. The orientation is given by the afore mentioned Colombo model. This is how our second equation, the one of Colombo, comes into play:

$$\frac{d\mathbf{k}}{dt} = \alpha(\hat{\mathbf{k}} \cdot \hat{\mathbf{n}})(\hat{\mathbf{k}} \times \hat{\mathbf{n}}). \tag{57}$$

All in all, we have to integrate the system (55–57). Table 4 gives the initial conditions used for integrating (57), while Table 5 gives the numerical values used for the parameters

Table 2 The orbital elements values taken as initial conditions for our simulations

Parameters	Numerical values
a	23459 km
e	0.0005
i	0.5 deg and 89 deg
Ω	10 deg
ω	5 deg
M	0 deg

Table 3 The initial positions and velocities used for Deimos. The first two rows correspond to the low-inclination case (0.5 degree); the last two rows correspond to the high-inclination case (89 degrees)

Satellite	x	y	z
Position km ($i = 0.5$)	22648.3376439	6068.52353055	17.8332361962
Velocity km/s ($i = 0.5$)	−0.349882011871	1.30576017694	$1.175229063323 \times 10^{-2}$
Position km ($i = 89$)	22996.9921622	4091.20549954	2043.25303109
Velocity km/s ($i = 89$)	−0.120115009144	$2.686751629968 \times 10^{-3}$	1.34652528539

Table 4 Initial conditions used for the integration of Eq. 57. These values were calculated based on Ward (1974)

Parameters	Numerical values
$I_p(t_0)$	25.25797549 deg
$h_p(t_0)$	332.6841708 deg

Table 5 Parameter values used in our simulations

Parameters	Numerical values
Martian mass (GM)	$42830\,\text{km}^3\ \text{s}^{-2}$
J_2	1960.45×10^{-6}
Equatorial radius	3397 km
Deimos mass	$0.091 \times 10^{-3}\,\text{km}^3\ \text{s}^{-2}$
α	3.9735×10^{-5} rad/yr

involved. It is worth noting that the values of Table 4 were calculated based on Ward (1974).

The software used for numerical integration of the system (55–57) is called NOE (Numerical Orbit and Ephemerides), and is largely based on the ideas and methods developed in Lainey et al. (2004). This numerical tool was created at the Royal Observatory of Belgium mainly for computations of the natural satellite ephemerides. It is an N-body code, which incorporates highly sensitive modelling and can generate partial derivatives. The latter are needed when one wants to fit the initial positions, velocities, and other parameters to the observation data. To save the computer time, an optimised force subroutine was built into the code, specifically for integrating the above equations. This appliance, based on the RA15 integrator offered by Everhart (1985), was chosen for its speed and accuracy. During the integration, a variable step size with an initial value of 0.04 day was used. To control the numerical error, back and forth integrations were performed. In particular, we carried out a trial simulation consisting of a thousand-year forward and a subsequent thousand-year back integration. The satellite displacement due to the error accumulated through this trial was constrained to 150 m. Most of this 150 m difference comes from a numerical drift of the longitude, while the numerical errors in the computation of the semi-major axis, the eccentricity, and the inclination were much lower. These errors were reduced for this trial simulation to only 10^{-5} km, 10^{-10}, and 10^{-10} degree, respectively. This provided us with a high confidence in our subsequent numerical results.

As a complement to the said back-and-forth check, the energy-conservation criterium was used to deduce, in the first approximation, an optimal initial step-size value and to figure out the numerical error proliferation. (It is for this energy-conservation test that we introduced a non-zero mass for Deimos. Its value was taken from Smith et al. (1995).) Applicability of this criterium is justified by the fact that the numerical errors are induced mostly by the fast orbital motion of the satellite.[5]

[5] Although the planet-satellite system is subject to an external influence (the solar torque acting on the planet), over short time scales this system can be assumed closed. In order to check the integrator efficiency and to determine an optimal initial step size, we carried out auxiliary integrations of (55)–(56), with the Colombo equation (57) neglected and with the energy presumed to conserve. These several-thousand-year-long trial integrations, with the energy-conservation criterium applied, led us to the conclusion that our integrator remained steady over long time scales and that the initial step of 0.04 day was optimal. Then this initial step size was employed in our integration of the full system (55)–(57).

3.2 Integration by the semianalytical approach

The theory of satellite-orbit evolution, based on the planetary equations whose right-hand sides combine those of (1–5) and (45), is semianalytical. This means that these equations for the elements' secular parts are derived analytically, but their integration is to be performed numerically. This integration was carried out using an 8^{th}-order Runge-Kutta scheme with relative and absolute tolerances of 10^{-12}. Kilograms, years, and kilometers were taken as the mass, time, and length units, correspondingly.

3.2.1 Technicalities

To integrate the planetary equations, one should know, at each time step, the values of $\dot{I}_p$ and $\dot{h}_p$, which are the time derivatives of the inclination and of the longitude of the node of the equator of date with respect to the equator of epoch. These derivatives will be rendered by the Colombo equation (17), after formulae (15–16) get inserted therein:

$$\begin{aligned}\dot{I}_p = -\alpha \Big(& q^2 \sin I_p \sin h_p \cos h_p - qp \sin I_p + 2pq \sin I_p \cos^2 h_p \\ & - p^2 \sin I_p \cos h_p \sin h_p + q\sqrt{1-q^2-p^2} \cos I_p \cos h_p \\ & - p\sqrt{1-q^2-p^2} \cos I_p \sin h_p \Big), \end{aligned} \tag{58}$$

and

$$\begin{aligned}\dot{h}_p = -\alpha \Bigg\{ & \left[\left(p - 2p\cos^2 I_p\right) \cos h_p + \frac{\left(-q + 2q\cos^2 I_p\right)\cos^2 h_p - 2q\cos^2 I_p + q}{\sin h_p} \right] \\ & \times \frac{\sqrt{1-p^2-q^2}}{\sin I_p} + \left(q^2 - p^2\right) \cos I_p \cos^2 h_p + \left(-p^2 - 2q^2 + 1\right) \cos I_p \\ & + \frac{2qp \cos I_p \cos^3 h_p - 2pq \cos h_p \cos I_p}{\sin h_p} \Bigg\}. \end{aligned} \tag{59}$$

Equations (58) and (59) are then integrated (with the initial conditions $I_p(t_0)$ and $h_p(t_0)$ borrowed from Table 4) simultaneously with the planetary equations (1–5). Through formulae (6), the above expressions for $\dot{I}_p$ and $\dot{h}_p$ yield the expressions for the components of $\boldsymbol{\mu}$. As can be seen from (12–14), integration of the planetary equations also requires the knowledge of the derivatives $\dot{\mu}_1$, $\dot{\mu}_2$, and $\dot{\mu}_3$ at each integration step. These can be readily obtained by differentiating (6). The resulting closed-formed expressions for $\dot{\mu}_1, \dot{\mu}_2, \dot{\mu}_3$ are listed in Appendix A. The final step required for numerical integration of the planetary equations is substitution of formulae (9–11), with the initial conditions from Table 2.

3.2.2 The plots and their interpretation

Figure 2 depicts the history of the planetary equator, in the Colombo approximation, over 1 Byr. The inclination exhibits long-periodic oscillations bounded within the range of 20.3 deg $\leq I_p \leq$ 30.3 deg, while the node regresses at a rate of $\dot{h}_p = 0.00202$ deg /yr. The obliquity, ϵ, varies in the range 15.2 deg $\leq \epsilon \leq$ 35.5 deg. A magnified view of the obliquity for 5 Myr is shown in Fig. 3. The time history of the obliquity closely matches the results reported by Ward (1974).

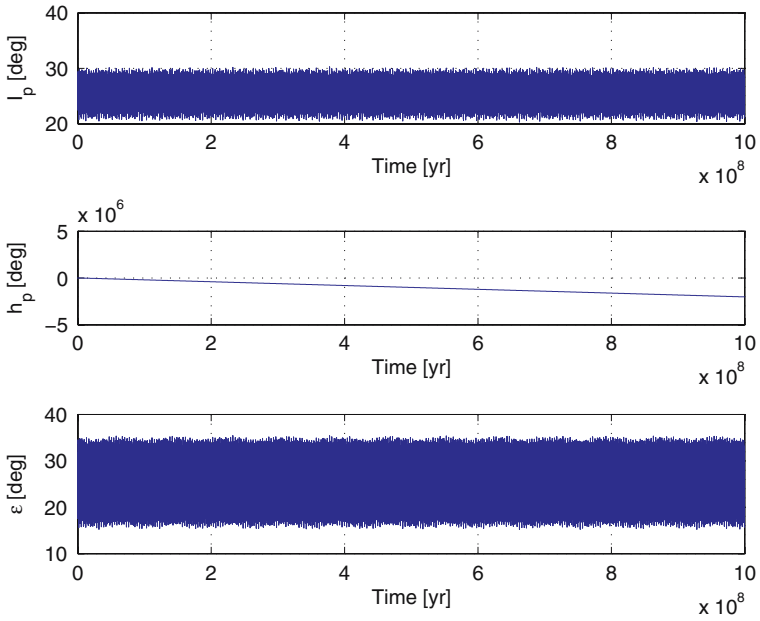

Fig. 2 Evolution of the Martian inclination, the longitude of the node of the equator of date relative to that of epoch, and the obliquity over 1 Byr, obtained in the Colombo approximation

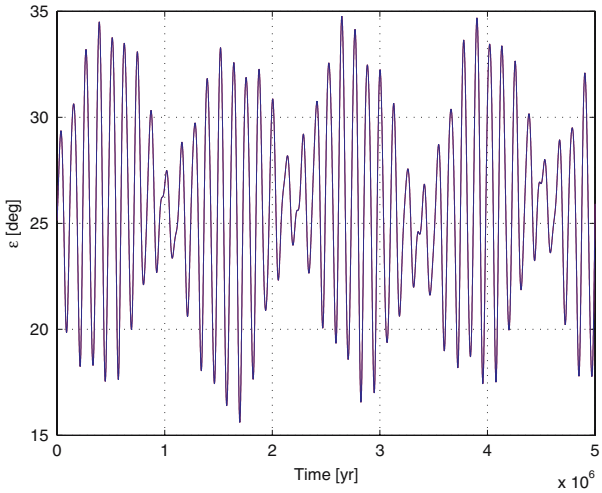

Fig. 3 Evolution of the the Martian obliquity for 5 Myr, calculated through formula (47). This curve closely matches the result of Ward (1974)

Integration of our semianalytical model gives plots depicted in Figs. 4 and 5, for a low initial inclination, and in Figs. 6–7, for a high initial inclination. From Fig. 4 we see that the variable equinoctial precession does not inflict considerable changes upon the satellite's inclination relative to the precessing equator of date. The orbit inclination remains bounded within the region 0.3 deg $\leq i \leq$ 2.5 deg. This means that the "Goldreich lock" (inclination

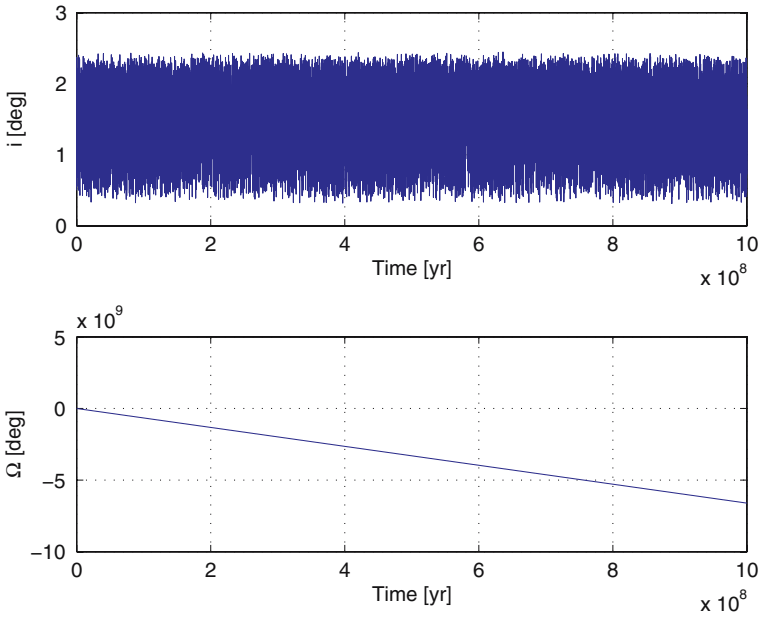

Fig. 4 Evolution of the inclination (initially set to 0.5 degree) and of the longitude of the node of Deimos over 1 Byr. The plot, obtained by integration of the semianalytical model, exhibits inclination locking and a uniform regression of the node

"locking," predicted by the Goldreich (1965) model for small inclinations and for uniform equinoctial precession) works also for nonuniform Colombo precession of the equator.

However, this observation no longer holds for large initial inclinations. In the $i_0 = 89$ deg case, it is clearly seen that the node is greatly affected by the presence of the equinoctial precession. The equinoctial precession also affects the magnitude of the inclination variations. This case exhibits chaotic dynamics that are sensitive to any additional perturbing inputs. Figure 6 shows that without precession the inclination of Deimos' orbit varies within the range of 84.5 deg $\leq i \leq$ 95 deg. With the precession included, the inclination gains about one degree in amplitude, varying in the range 83.5 deg $\leq i \leq$ 96 deg. This effect is accentuated when examining a magnification of the inclination over a 5 Myr span, as shown in Fig. 6. The chaotic nature of the inclination is clearly seen. The irregular dynamics is characterised by chaotic switches between the maximum and minimum inclination values, a phenomenon referred to as "crankshaft", to be further discussed in the sequel.

Both in the near-equatorial case (as in Fig. 5) and the near-polar case (as in Fig. 7), variations of the semimajor axis are of order 10^{-6}%. This smallness is in compliance with formula (44) in Efroimsky (2006a, b), according to which the changes of a generated by the variations of the equinoctial precession rate are extremely small. (Formula (38a) from Subsect. 2.4 above tells us that the direct pull of the Sun exerts no influence upon a at all.)

Similarly, in both cases (Figs. 5 and 7) the variations of eccentricity, remain small, about 10^{-3}%. While formula (44) in Efroimsky (2006a, b) promises to e only tiny variations due to precession, our formula (38b) from Subsect. 2.4 above gives to e a slightly higher variation rate, rate that still remains insufficient to raise the quasiperiodic changes in e above a fraction of percent.

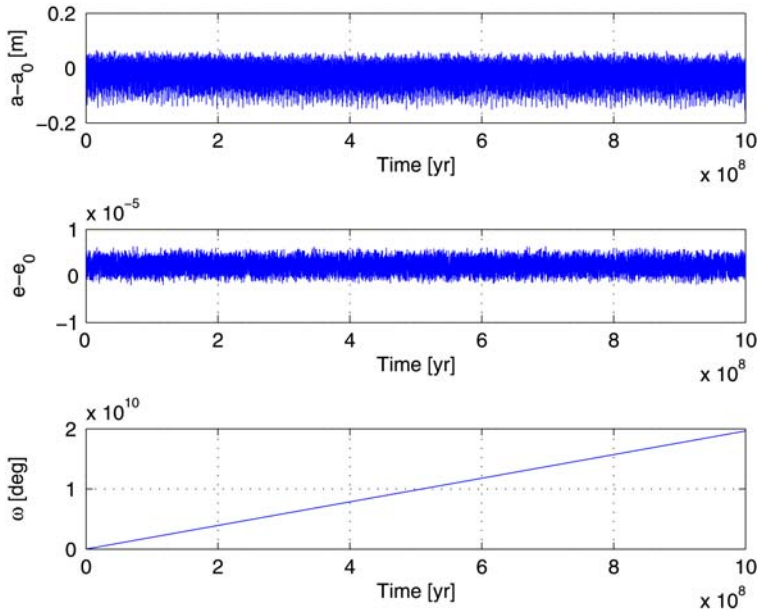

Fig. 5 Evolution of the semimajor axis, eccentricity, and argument of periapsis of Deimos over 1 Byr. (The inclination was initially set to 0.5 degree.) Both the semimajor axis and eccentricity exhibit quasiperiodic motion about their initial values. (The variations of the semimajor axis and eccentricity are so small that it is more convenient to plot $a - a_0$ and $e - e_0$.) The plots were obtained by integration of the semianalytical model

The plots in Figs. 5 and 7 depict also the time evolution of ω. The line of apsides steadily regresses in the near-polar case and steadily advances in the near-equatorial case.

To examine the precision of our semianalytical model, we have compared the results of its integration with the results stemming from a purely numerical simulation performed in terms of inertial Cartesian coordinates and velocities (see Subsect. 3.1). The necessity for this check was dictated, mainly, by the fact that within the semianalytical model the short-period terms are averaged out,[6] while the straightforward numerical integration of (55–56) neglects nothing. We carried out comparison of the two methods over 10 Myr only. The outcomes, both for $i_0 = 0.5$ degrees and $i_0 = 89$ deg, were in a good agreement. As an example, the top plot in Fig. 8 shows the comparison of the inclination evolution calculated by the semianalytical and purely numerical methods over 10 Myr in the case of $i_0 = 0.5$ deg. The bottom plot in Fig. 8 depicts a similar comparison for the case of $i_0 = 89$ deg. Since the inclination exhibits chaotic behaviour, comparing the semianalytical and purely numerical calculations point-by-point (i. e., computing the differences between these two signals) would not be useful. Therefore, we chose to compare the mean and standard deviation (STD) of the inclination, in the semianalytical and purely numerical simulations. We also compared the extremum values. The results of this comparison are summarised by Table 6. The table quantifies the agreement between the models depicted by Fig. 8. It clearly demonstrates that the two simulations agree up to fractions of a percent.

[6] We remind that in equations (1–5) the exact $\boldsymbol{\mu}$-dependent terms are substituted with their orbital averages (12–14).

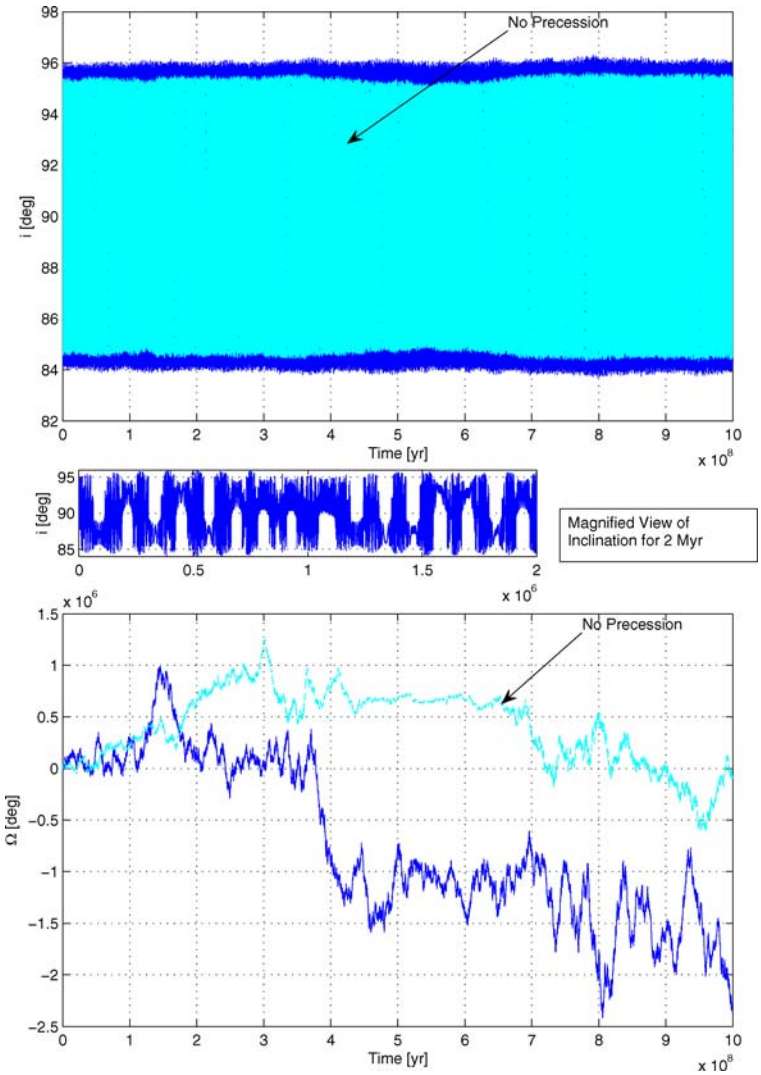

Fig. 6 Evolution of the inclination and of the longitude of the node of Deimos over 1 Byr. (The inclination was initially set to 89 degrees.) The plot, obtained by integration of the semianalytical model, exhibits inclination variation in the range ± 5 deg and a chaotic evolution of the node; if precession is neglected, the inclination oscillations are smaller in magnitude. The chaotic nature of the inclination variation is referred to as "crankshaft chaos"

All in all, the outcome of our computations is two-fold. First, we have made sure that the semianalytical model perfectly describes the dynamics over time scales of, at least, dozens of millions of years. Stated differently, the short-period terms and the terms of order $O(\mu^2)$ play no role over these time spans. Second, we have made sure that the "Goldreich lock" initially derived for very low inclinations and for uniform equinoctial precession, works well also for variable precession, though for low initial inclinations only.

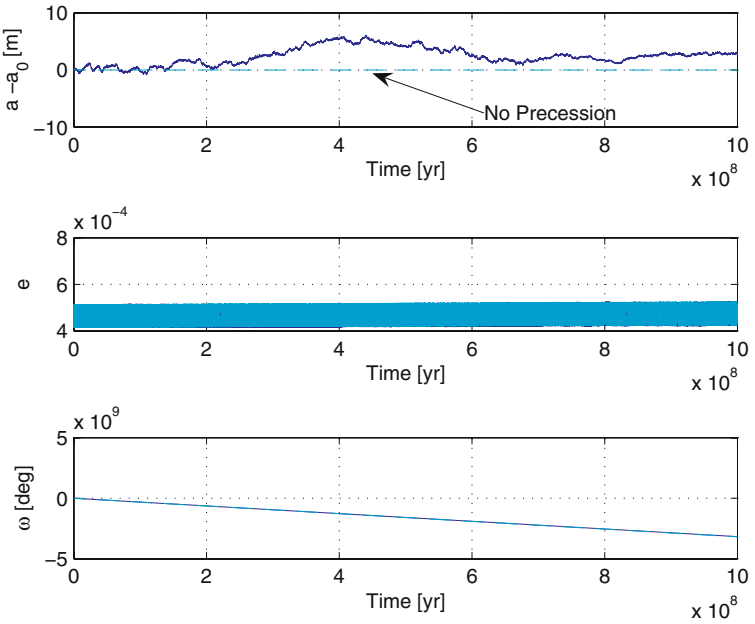

Fig. 7 Evolution of the semi-major axis, eccentricity, and argument of periapsis of Deimos over 1 Byr. (The inclination was initially set to 89 degrees.) The semi-major axis exhibits chaotic behavior and the eccentricity exhibits long-periodic motion about the initial value. (The variations of the semimajor axis are so small that it is more convenient to plot $a - a_o$ rather than a.) The plots were obtained by integration of the semianalytical model

Table 6 Statistical properties of the inclination. Comparison of the results of the semianalytical and the purely numerical computation

i_0 [deg]	Model	STD [deg]	Mean [deg]	Max. value [deg]	Min. value [deg]
0.5	Semianalytical	0.60	1.519	2.45	0.3063
	Cartesian	0.601	1.53	2.465	0.3056
89	Semianalytical	3.10	90.085	95.9713	84.027
	Cartesian	3.09	89.92	95.9769	84.0054

3.2.3 Looking for trouble

A natural question arises as to whether the considered examples are representative. One may enquire if, perhaps, there still exists a combination of the initial conditions yielding noticeable variations of the satellite orbit inclination during the primary's variable equinoctial precession over vast spans of time. To answer this question, we should scan through all the possible combinations of initial conditions, to identify a particular combination that would entail a maximal inclination excursion relative to the initial inclination (Gurfil et al. 2002). Stated more formally, we should seek a set of initial conditions $\{h^\star_{p0}, I^\star_{p0}, i^\star_0, \Omega^\star_0, \omega^\star_0\}$ maximising the objective function $|i(t) - i_0|$:

$$\{h^\star_{p0}, I^\star_{p0}, i^\star_0, \Omega^\star_0, \omega^\star_0\} = \underset{\substack{t, h_{p0}, I_{p0} \\ i_0, \Omega_0, \omega_0}}{\arg\max} |i(t) - i_0| \tag{60}$$

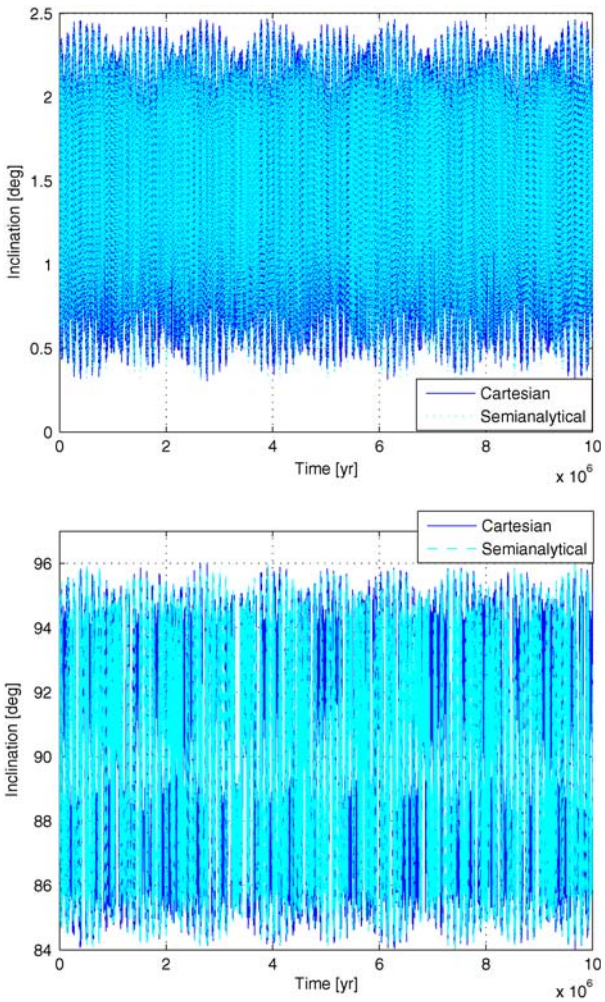

Fig. 8 Comparison of the semi-analytical model to a purely numerical integration. The plot shows the inclination as predicted by the two models. The top plot shows the case of the initial inclination $i_0 = 0.5$ deg. In this case, the standard deviation of the inclination in the semianalytical and inertial models differs by 0.175%, and the mean value by 0.77%. The bottom plot shows the case of the initial inclination $i_0 = 89$ deg. In this case, the differences between the semianalytical and the numerical model amount to 0.4% in standard deviation and 0.18% in the mean value

This problem belongs to the realm of optimisation theory. The optimisation space is constituted by the entire multitude of the permissible initial conditions. The sought after combination of initial conditions will be called *the optimal set*.

In this situation, the traditional optimisation schemes (such as the gradient search or the simplex method) may fail due to the rich dynamical structure of our problem—these methods may lead us to a local extremum only. Thus, the search needs to be global. It can be carried out by means of Genetic Algorithms (GA's) (Goldberg 1989; Gurfil et al. 2002; Gurfil and Kasdin 2002a, b). These are wont to supersede the traditional optimisation procedures in the following aspects. First, instead of directly dealing with the parameters, the GA's employ

Table 7 Parameter values used for the GA optimization

Parameters	Numerical values
Population size	30
Number of generations	100
String length	16 bit
Probability of crossover	0.99
Probability of mutation	0.02

codings (usually, binary) of the parameter set ("strings," in the GA terminology). Second, instead of addressing a single point of the optimisation space, the GAs perform a search inside a population of the initial conditions. Third, instead of processing derivatives or whatever other auxiliary information, the GAs use only objective-function evaluations ("fitness evaluations"). Fourth, instead of deterministic rules to reiterate, the GAs rely upon probabilistic transition rules. Additional details on the particular GA mechanism used herein can be found in Appendix B.

A GA optimisation was implemented using the parameter values given in Table 7.

The search for the inclination-maximising initial conditions resulted in the following set:

$$I_{p0}^{\star} = 72.5 \text{ deg}, \quad h_{p0}^{\star} = 211.324 \text{ deg}, \quad i_0^{\star} = 100.543 \text{ deg},$$
$$\Omega_0^{\star} = 111.538 \text{ deg}, \quad \omega_0^{\star} = 234.913 \text{ deg}. \tag{61}$$

Thus, the initial orbit is *retrograde* and, not surprisingly, *near-polar*. The resulting time histories for a 0.2 Byr integration are depicted in Fig. 9, for i and Ω. In both cases the inclination amplitude is relatively large: The inclination varies within the range of 79 deg $< i <$ 102 deg.

This example clearly shows that the equinoctial precession is an important effect for evolution of satellite orbits. As shown in the upper pane of Fig. 9, had we neglected the precession, the magnitude of the oscillations would be about twice smaller. The inclusion of the precession in the model qualitatively modifies the behavior, inducing large-magnitude chaotic variations of the inclination, a phenomenon that cannot be detected without including the precession alongside the oblateness and solar gravity.

4 Comparison of the semianalytical results with those rendered by Goldreich's model

The final step in our study will be to compare the semianalytical model to Goldreich's approximation (22–26). To that end, we integrate our semianalytical model for 20 Myr, using the initial conditions from Table 2 with $i_0 = 89$ deg; and compare the outcome with that resulting from Goldreich's approximation simulated with the same initial conditions. The results of this comparison are depicted in Figs. 10 and 11. Specifically, Fig. 10 compares the time histories of I_p and h_p. There are noticeable differences in the dynamics of I_p. While Goldreich's approximation assumes a constant I_p, the semianalytical model is based on the Colombo calculation of the equinoctial precession, calculation that predicts considerable oscillations within the range 21 deg $\leq I_p \leq$ 30 deg. Beside this, in our semianalytical model we take into account the direct gravitational pull exerted by the Sun on the satellite. All this entails differences between the dynamics predicted by our semianalytical model and the dynamics stemming from the Goldreich approximation. These differences, for i and Ω, are depicted in Fig. 11. In Goldreich's model, i stays very close to the initial value: 88.27 deg $\leq i \leq$ 89.01 deg, a behaviour that makes the essence of the *Goldreich lock*. However, in the more accurate, semianalytical model we have 84 deg $\leq i \leq$ 96 deg. The time history of Ω, too, reveals that

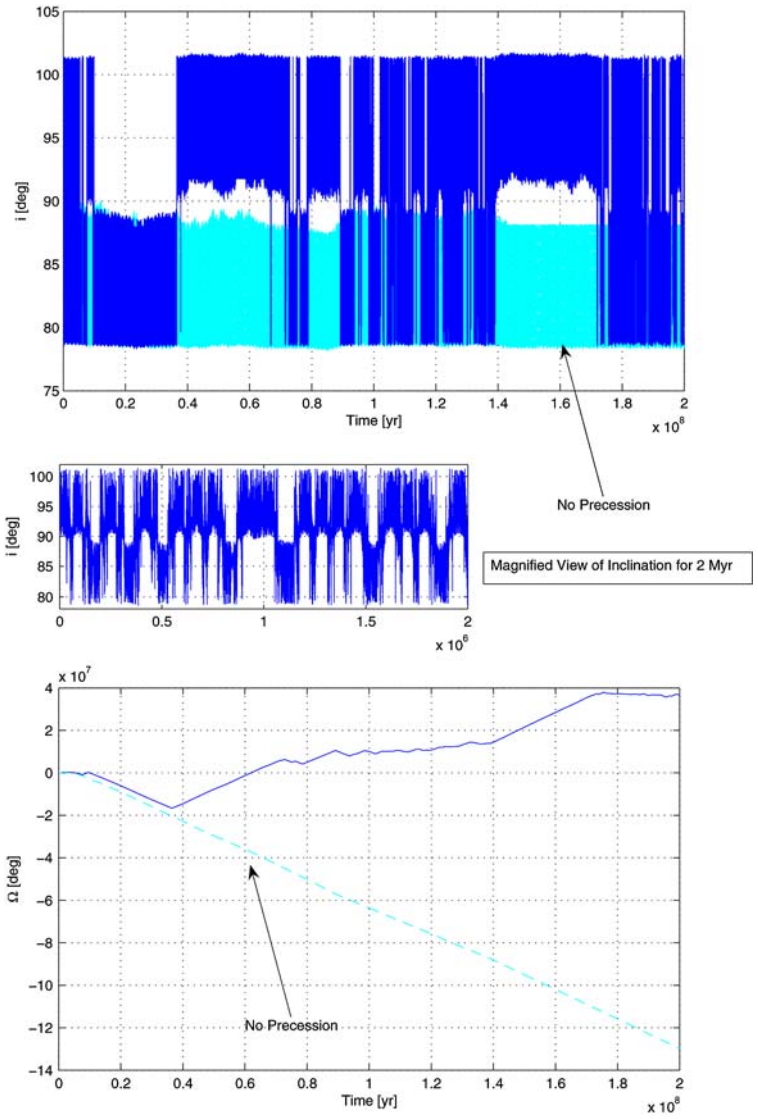

Fig. 9 Evolution of the inclination and longitude of the node, for the initial conditions that entail maximal variations of the orbit inclination. The plot, obtained by integration of the semianalytical model, demonstrates that the inclination, initially set at 100.5 deg, plunges to less than 80 deg and then returns to its initial value. The switches between maximum and minimum values exhibit "crankshaft" chaos. Without precession, the inclination magnitude is much smaller, and the node regresses uniformly

Goldreich's approximation does not adequately model the actual dynamics, since it predicts a much larger secular change than the semi-analytical model.

All in all, the dynamics (i.e., particular trajectories) predicted by the two models are quantitatively different. At the same time, when it comes to the most physically important conclusion from the Goldreich approximation, the "Goldreich lock" of the inclination, one may still say that, qualitatively, the semianalytical model confirms the locking even in the case

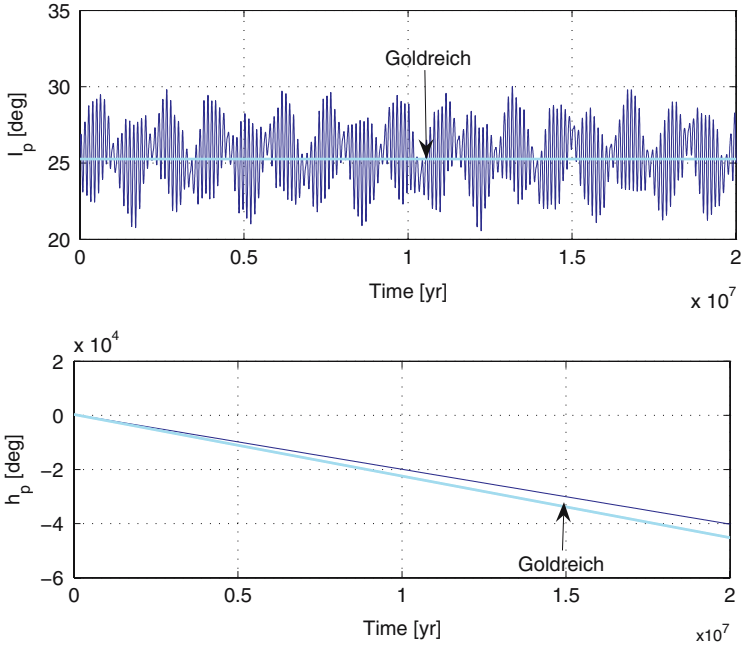

Fig. 10 Preparation to comparison of the semianalytical model to Goldreich's model. In Goldreich's model, the Martian equator is assumed to precess uniformly, while the semianalytical model takes into account (via Colombo's equation) variations of the equinoctial precession

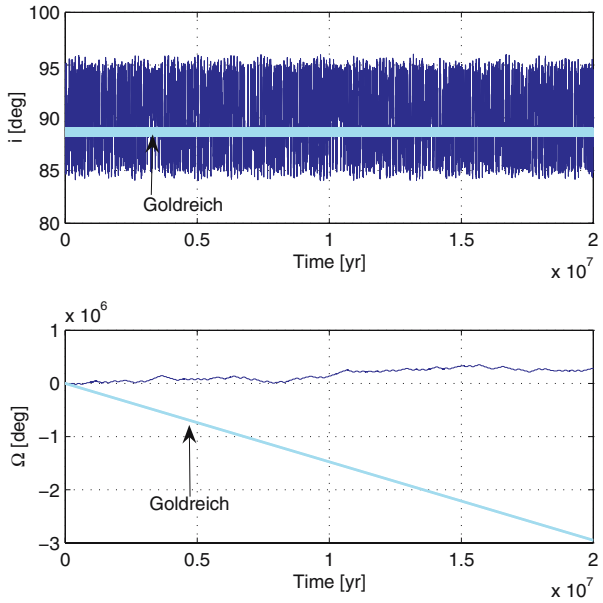

Fig. 11 Comparison of the semi-analytical model to Goldreich's model for a satellite of Deimos' mass and with the initial conditions given by (61). While in Goldreich's model the inclination remains tightly locked, the semianalytical model reveals much larger variations of i

when the equinoctial precession is variable, and the solar pull on the satellite is included. The locking survives even for highly inclined satellite orbits. It is, though, not as stiff as predicted by the Goldreich model: we can see from Fig. 11 that the orbit inclination varies within a five-degree span, while the Goldreich approximation would constrain it to fractions of a degree.

An intriguing fine feature of the inclination evolution, which manifests itself for orbits close to polar, is the "crankshaft". This kind of behaviour, well defined in Fig. 11, is not rendered by the Goldreich model, because that model was initially developed for small inclinations and uniform precession. One might suspect that the "crankshaft" is merely a numerical artefact, had it not been discovered under different circumstances (in the absence of precession but in the presence of a third body) by Zhang and Hamilton (2005). This kind of pattern may be generic for the close vicinity of $i = 90$ deg.

5 Conclusions

In the article thus far, we continued developing a tool for exploring long-term evolution of a satellite orbit about a precessing oblate primary. In particular, we were interested in the time-dependence of the orbit inclination relative to the moving equator of date. Our model includes three factors: J_2 of the planet, the planet's nonuniform equinoctial precession described by the Colombo formalism, and the gravitational pull exerted by the Sun on the satellite. The problem was approached using different methods. One, semianalytical, was based on numerical integration of the averaged Lagrange-type equations for the secular parts of the Keplerian orbital elements introduced in a noninertial reference frame coprecessing with the planetary equator of date. The right-hand sides of these equations consisted of precession-generated contributions and contributions due to the direct pull of the Sun. The other approach was a straightforward, purely numerical, computation of the satellite dynamics using Cartesian coordinates in a quasi-inertial reference frame.

The results of both computations have demonstrated a good agreement over 10 Myr. This means that the semianalytical model adequately describes the dynamics over this time span. Specifically, the terms neglected in the semianalytical model (the short-period terms and the terms of order $O(\mu^2)$) play no significant role on this time scale.

Our calculations have shown the advantages and the limitations of a simple model developed by Goldreich (1965) for uniform equinoctial precession and low inclinations. Though his model does not adequately describe the dynamics (that turns out to be chaotic), the main physical prediction of Goldreich's model—the "Goldreich lock"—sustains the presence of the Sun and variations of equinoctial precession, provided the initial inclination is sufficiently low. For low initial inclinations, the inclination exhibits variations of order fractions of a degree. For higher inclinations, however, it varies already within a span of about ten degrees. For near-polar orbits, the inclination behaviour demonstrates the "crankshaft", an chaotic pattern not accounted for by the Goldreich model. The "crankshaft" emerges because in our model both the precession variations and the pull of the Sun are included into the model. However, numerical experiments have also shown that the "crankshaft" gets generated by each of these two factors separately.

Acknowledgements ME is grateful to George Kaplan for numerous fruitful discussions on the subject, and to Marc Murison for a consultation on the possible scenario of the Martian satellites capture. The work of ME was partially supported by NASA grant W-19948. The work of VL was supported by the European Community's Improving Human Potential Programme contract RTN2-2001-00414 MAGE.

Appendix A: Closed-form expressions for $\dot{\mu}_1, \dot{\mu}_2, \dot{\mu}_3$

Using the compact notation $\mathrm{c}_{(\cdot)} \equiv \cos(\cdot)$ and $\mathrm{s}_{(\cdot)} \equiv \sin(\cdot)$, and conforming to the procedure described in the text, we obtain the following expressions for $\dot{\mu}_1, \dot{\mu}_2, \dot{\mu}_3$:

$$
\begin{aligned}
\dot{\mu}_1 = {} & (((6\,p^2q^2 - p^4 - q^4)(\mathrm{c}_{I_p})^3 + (-6\,p^2q^2 + p^4 + q^4)\mathrm{c}_{I_p})(\mathrm{c}_{h_p})^4 \\
& + ((-3\,p^4 - 6\,p^2q^2 - 3\,q^2 + 3\,p^2 + 5\,q^4)(\mathrm{c}_{I_p})^3 \\
& + (2\,p^4 - 4\,q^4 + 6\,p^2q^2 - 2\,p^2 + 2\,q^2)\mathrm{c}_{I_p}) \cdot (\mathrm{c}(h_p))^2 \\
& + (3\,q^2 - 3\,p^2q^2 - 4\,q^4)(\mathrm{c}_{I_p})^3 + (3\,q^4 - 2\,q^2 + 2\,p^2q^2)\mathrm{c}_{I_p} \\
& + (((4\,qp^3 - 4\,q^3p)(\mathrm{c}_{I_p})^3 + (4\,q^3p - 4\,qp^3)\mathrm{c}_{I_p})(\mathrm{c}_{h_p})^5 \\
& + ((2\,qp^3 - 6\,qp + 14\,q^3p)(\mathrm{c}_{I_p})^3 \\
& + (-12\,q^3p + 4\,qp)\mathrm{c}_{I_p})(\mathrm{c}_{h_p})^3 + ((6\,qp - 10\,q^3p - 6\,qp^3)(\mathrm{c}_{I_p})^3 \\
& + (4\,qp^3 + 8\,q^3p - 4\,qp)\mathrm{c}_{I_p})\mathrm{c}_{h_p}) \cdot (\mathrm{s}_{h_p})^{-1})(\mathrm{s}_{I_p})^{-1} \\
& + ((-9\,pq^2 + 9\,pq^4 - 3\,p^5 + 3\,p^3 + 6\,p^3q^2)(\mathrm{c}_{I_p})^2 + 3\,pq^2 - 2\,p^3q^2 + p^5 \\
& - 3pq^4 - p^3)(\mathrm{c}_{h_p}^3 + ((-11\,p^3q^2 - p^5 - 10\,pq^4 - p + 2\,p^3 + 11\,pq^2)(\mathrm{c}(I_p))^2 \\
& + 3pq^4 + 3\,p^3q^2 - 3pq^2)\mathrm{c}_{h_p} + (((-9\,p^2q + 6\,p^2q^3 + 9\,p^4q - 3\,q^5 + 3\,q^3)(\mathrm{c}_{I_p})^2 \\
& - 3\,p^4q + 3\,p^2q - 2\,p^2q^3 \\
& - q^3 + q^5)(\mathrm{c}_{h_p}^4 + ((7\,p^2q - p^2q^3 - 8\,q^3 - 8\,p^4q + 7\,q^5 + q)(\mathrm{c}_{I_p})^2 \\
& - 2q^5 + p^2q^3 + 2\,q^3 \\
& + 3p^4q - 3\,p^2q)(\mathrm{c}(h_p))^2 + (5\,q^3 - 4\,q^5 - q - 5\,p^2q^3 - p^4q + 2\,p^2q)(\mathrm{c}_{I_p})^2 \\
& - q^3 + q^5 + p^2q^3) \cdot \left(\mathrm{s}(h_p))^{-1}\right)\left[\sqrt{1 - p^2 - q^2}\right]^{-1}\Bigg)\alpha^2 \\
& - \alpha\Bigg(((-2\,q\,\dot{p} - 2\,\dot{q}\,p)(\mathrm{c}_{I_p})^2 + 2\,q\,\dot{p} + 2\,\dot{q}\,p)(\mathrm{c}_{h_p})^2 \\
& + (\dot{q}\,p + q\,\dot{p})(\mathrm{c}_{I_p})^2 - \dot{q}\,p - q\,\dot{p} + (((-2\,p\,\dot{p} + 2\,q\,\dot{q})(\mathrm{c}_{I_p})^2 + 2\,p\,\dot{p} - 2\,q\,\dot{q})(\mathrm{c}_{h_p})^3 \\
& + ((2\,p\,\dot{p} - 2\,q\,\dot{q})(\mathrm{c}_{I_p})^2 - 2\,p\,\dot{p} + 2\,q\,\dot{q})\mathrm{c}_{h_p})(\mathrm{s}(h_p))^{-1})(\mathrm{s}(I_p))^{-1} \\
& + \Bigg((-\dot{q}\,p^2 - 2\,q^2\dot{q} + \dot{q} - qp\,\dot{p})\mathrm{c}_{I_p}\mathrm{c}_{h_p} \\
& + \frac{(\dot{p} - 2\,p^2\dot{p} - pq\dot{q} - \dot{p}\,q^2)\mathrm{c}_{I_p}(\mathrm{c}_{h_p})^2 + (-\dot{p} + \dot{p}\,q^2 + 2\,p^2\dot{p} + pq\dot{q})\mathrm{c}_{I_p}}{\mathrm{s}_{h_p}}\Bigg) \\
& \left[\sqrt{1 - p^2 - q^2}\right]^{-1}\Bigg), \qquad (62)
\end{aligned}
$$

$$
\begin{aligned}
\dot{\mu}_2 = {} & \Bigg(((4\,q^3p - 4\,qp^3)(\mathrm{c}_{I_p})^2 + 4\,qp^3 - 4\,q^3p)(\mathrm{c}_{h_p})^4 \\
& + ((qp^3 - 7\,q^3p + 2\,qp)(\mathrm{c}_{I_p})^2 - 3\,qp^3 + 5\,q^3p)(\mathrm{c}_{h_p})^2 \\
& + (2\,q^3p - qp + qp^3)(\mathrm{c}_{I_p})^2 - q^3p + (((6\,p^2q^2 - p^4 - q^4)(\mathrm{c}_{I_p})^2
\end{aligned}
$$

$$
\begin{aligned}
&-6p^2q^2+p^4+q^4)(\mathrm{c}_{h_p}^5+((3q^4-q^2-9\,p^2q^2+p^2)(\mathrm{c}_{I_p})^2\\
&-p^4-2q^4+9\,p^2q^2)(\mathrm{c}_{h_p})^3+((-p^2+q^2-2q^4+p^4+3\,p^2q^2)(\mathrm{c}(I_p))^2\\
&+q^4-3\,p^2q^2)\mathrm{c}(h_p))(\mathrm{s}_{h_p})^{-1})(\mathrm{s}(I_p))^{-1}+((-4\,p^2q^3+6\,p^2q-2q^3\\
&+2q^5-6\,p^4q)\mathrm{c}(I_p)(\mathrm{c}_{h_p})^3+(2q^3+4\,p^4q+2\,p^2q^3-4\,p^2q-2q^5)\mathrm{c}_{I_p}\mathrm{c}_{h_p}\\
&+((-2\,p^5-6\,pq^2+6\,pq^4+4\,p^3q^2+2\,p^3)\mathrm{c}_{I_p}(\mathrm{c}_{h_p})^4\\
&+(2\,p^5+8\,pq^2-8\,pq^4-6\,p^3q^2-2\,p^3)\mathrm{c}_{I_p}(\mathrm{c}_{h_p})^2+(2\,pq^4-2\,pq^2\\
&+2\,p^3q^2)\mathrm{c}_{I_p})(\mathrm{s}_{h_p})^{-1})\cdot\left[\sqrt{1-p^2-q^2}\right]^{-1}\Bigg)\alpha^2\\
&-\alpha((2\,p\dot{p}-2\,q\dot{q})(\mathrm{c}_{I_p})^3+(-2\,p\dot{p}+2\,q\dot{q})\mathrm{c}_{I_p})(\mathrm{c}_{h_p}^2\\
&+(2\,p\dot{p}+4\,q\dot{q})(\mathrm{c}_{I_p})^3+(-2\,p\dot{p}-4\,q\dot{q})\mathrm{c}_{I_p}+(((-2\,q\dot{p}-2\,\dot{q}\,p)(\mathrm{c}_{I_p})^3\\
&+(2\,q\dot{p}+2\,\dot{q}\,p)\mathrm{c}_{I_p})(\mathrm{c}_{h_p})^3+((2\,q\dot{p}+2\,\dot{q}\,p)(\mathrm{c}(I_p))^3\\
&+(-2\,q\dot{p}-2\,\dot{q}\,p)\mathrm{c}_{I_p})\mathrm{c}(h_p))(\mathrm{s}_{h_p})^{-1})(\mathrm{s}_{I_p})^{-1}\\
&+((2\,\dot{p}\,q^2+2\,pq\dot{q}+4\,p^2\dot{p}-2\,\dot{p})(\mathrm{c}_{I_p})^2+\dot{p}-2\,p^2\dot{p}-pq\dot{q}-\dot{p}\,q^2)\mathrm{c}_{h_p}\\
&+\Bigg(((-2\,qp\dot{p}-2\,\dot{q}\,p^2-4\,q^2\dot{q}+2\,\dot{q})(\mathrm{c}_{I_p})^2-\dot{q}+\dot{q}\,p^2+2\,q^2\dot{q}+qp\dot{p})(\mathrm{c}_{h_p}^2\\
&+(2\,qp\dot{p}-2\,\dot{q}+2\,\dot{q}\,p^2+4\,q^2\dot{q})(\mathrm{c}_{I_p})^2\\
&-\dot{q}\,p^2-2\,q^2\dot{q}+\dot{q}-qp\dot{p})\cdot(\mathrm{s}(h_p))^{-1}\left[\sqrt{1-p^2-q^2}\right]^{-1}\Bigg),
\end{aligned}
\tag{63}
$$

and

$$
\begin{aligned}
\dot{\mu}_3=&\Bigg((((4q^3p-4qp^3)(\mathrm{c}_{I_p})^2+4qp^3-4q^3p)(\mathrm{c}_{h_p})^4+((qp^3-7q^3p+2qp)(\mathrm{c}(I_p))^2\\
&-3qp^3+5q^3p)(\mathrm{c}_{h_p})^2+(2q^3p-qp+qp^3)(\mathrm{c}_{I_p})^2-q^3p\\
&+(((6\,p^2q^2-p^4-q^4)(\mathrm{c}_{I_p})^2-6\,p^2q^2+p^4\\
&+q^4)(\mathrm{c}(h_p))^5+((3q^4-q^2-9\,p^2q^2+p^2)(\mathrm{c}_{I_p})^2-p^4-2q^4+9\,p^2q^2)(\mathrm{c}_{h_p})^3\\
&+((-p^2+q^2-2q^4+\ p^4+3\,p^2q^2)(\mathrm{c}(I_p))^2+q^4-3\,p^2q^2)\mathrm{c}(h_p))(\mathrm{s}_{h_p})^{-1})(\mathrm{s}(I_p))^{-1}\\
&+((-4\,p^2q^3+6\,p^2q-2q^3+2q^5\\
&-6\,p^4q)\mathrm{c}(I_p)(\mathrm{c}_{h_p})^3+(2q^3+4\,p^4q+2\,p^2q^3-4\,p^2q-2q^5)\mathrm{c}_{I_p}\mathrm{c}_{h_p}\\
&+((-2\,p^5-6\,pq^2+6\,pq^4+4\,p^3q^2+2\,p^3)\mathrm{c}_{I_p}(\mathrm{c}_{h_p})^4\\
&+(2\,p^5+8\,pq^2-8\,pq^4-6\,p^3q^2-2\,p^3)\mathrm{c}_{I_p}(\mathrm{c}_{h_p})^2\\
&+(2\,pq^4-2\,pq^2+2\,p^3q^2)\mathrm{c}_{I_p})(\mathrm{s}_{h_p})^{-1})\sqrt{1-p^2-q^2}^{-1}\Bigg)\alpha^2-\alpha\Bigg(((2\,p\dot{p}-2\,q\dot{q})(\mathrm{c}_{I_p})^3\\
&+(-2\,p\dot{p}+2\,q\dot{q})\mathrm{c}(I_p))(\mathrm{c}(h_p))^2+(2\,p\dot{p}+4\,q\dot{q})(\mathrm{c}_{I_p})^3+(-2\,p\dot{p}-4\,q\dot{q})\mathrm{c}_{I_p}\\
&+(((-2\,q\dot{p}-2\,\dot{q}\,p)(\mathrm{c}_{I_p})^3+(2\,q\dot{p}+2\,\dot{q}\,p)\mathrm{c}_{I_p})(\mathrm{c}_{h_p})^3+((2\,q\dot{p}+2\,\dot{q}\,p)(\mathrm{c}(I_p))^3
\end{aligned}
$$

$$+(-2q\dot{p}-2\dot{q}\,p)\mathrm{c}_{I_p})\mathrm{c}(h_p))(\mathrm{s}_{h_p})^{-1})(\mathrm{s}_{I_p})^{-1}+(((2\dot{p}q^2+2pq\dot{q}+4p^2\dot{p}$$
$$-2\dot{p})(\mathrm{c}_{I_p})^2+\dot{p}-2p^2\dot{p}-pq\dot{q}$$
$$-\dot{p}q^2)\mathrm{c}_{h_p}+(((-2qp\dot{p}-2\dot{q}\,p^2-4q^2\dot{q}+2\dot{q})(\mathrm{c}(I_p))^2-\dot{q}+\dot{q}\,p^2+2q^2\dot{q}$$
$$+qp\dot{p})(\mathrm{c}_{h_p})^2+(2qp\dot{p}-2\dot{q}+2\dot{q}\,p^2+4q^2\dot{q})(\mathrm{c}_{I_p})^2-\dot{q}\,p^2$$
$$-2q^2\dot{q}+\dot{q}-qp\dot{p})(\mathrm{s}_{h_p})^{-1})\cdot\left[\sqrt{1-p^2-q^2}\right]^{-1}\Bigg) \tag{64}$$

Appendix B: Niching genetic algorithms

The most commonly used Genetic Algorithm (GA) is the so-called "Simple GA" (Goldberg 1989). To perform an evolutionary search, the Simple GA uses the operators of crossover, reproduction, and mutation. A crossover is used to create new solution strings ("children" or "offspring") from the existing strings ("parents"). Reproduction copies individual strings according to the objective function values. Mutation is an occasional random alteration of the value of a string position, used to promote diversity of solutions.

Although Simple GA's are capable of detecting the global optimum, they suffer from two main drawbacks. First, convergence to a local optimum is possible due to the effect of premature convergence, where all individuals in a population become nearly identical before the optima has been located. Second, convergence to a single optimum does not reveal other optima, which may exhibit attractive features. To overcome these problems, modifications of Simple GA's were considered. These modifications are called niching methods, and are aimed at promoting a diversity of solutions for multi-modal optimisation problems. In other words, instead of converging to a single (possibly local) optimum, niching allows for a number of optimal solutions to co-exist, and it lets the designer choose the appropriate one. The niching method used throughout this study is that of Deterministic Crowding. According to this method, individuals are first randomly grouped into parent pairs. Each pair generates two children by application of the standard genetic operators. Every child then competes against one of his parents. The winner of the competition moves on to the next generation. By using the notation P_i for a parent, C_i for a child, $f(\cdot)$ for a fitness, and $d(\cdot)$ for a distance, a pseudo-code for the two possible parent-child tournaments can be written as follows (Gurfil and Kasdin 2002a, b):

If $[d(P_1, C_1) + d(P_2, C_2) = d(P_1, C_2) + d(P_2, C_1)]$
If $f(C_1) \geq f(P_1)$ replace P_1 with C_1
If $f(C_2) \geq f(P_2)$ replace P_2 with C_2
Else
If $f(C_1) \geq f(P_2)$ replace P_2 with C_1
If $f(C_2) \geq f(P_1)$ replace P_1 with C_2

In addition to applying the Deterministic Crowding niching method, we used a two-point crossover instead of a single-point one. In the Simple GA, the crossover operator breaks the binary string of parameters, the "chromosome," at a random point and exchanges the two pieces to create a new "chromosome." In a two-point crossover, the "chromosome" is represented with a ring. The string between the two-crossover points is then exchanged. The two-point crossover or other multiple-point crossover schemes have preferable properties when optimisation highly nonlinear functions is performed.

References

Bills, B.G.: Non-chaotic obliquity variations of Mars. The 37th Annual Lunar and Planetary Science Conference, pp. 13–17, March 2006, League City, TX (2006)

Brouwer, D.: Solution of the problem of artificial satellite theory without drag. Astron. J. **64**, 378–397 (1959)

Brouwer, D., van Woerkom, A.J.J.: The secular variations of the orbital elements of the principal planets. Astronomical papers prepared for the use of the American Ephemeris and Nautical Almanac, vol. 13, Part 2, pp. 81–107. US Government Printing Office, Washington, DC (1950)

Brumberg, V.A., Evdokimova, L.S., Kochina, N.G.: Analytical methods for the orbits of artificial satellites of the moon. Celestial Mech. **3**, 197–221 (1971)

Burns, J.: Dynamical characteristics of phobos and deimos. Rev. Geophys. Space Phys. **6**, 463–483 (1972)

Burns, J.: The dynamical evolution and origin of the Martian moons. Vistas Astron. **22**, 193–210 (1978)

Colombo, G.: Cassini's second and third laws. Astron. J. **71**, 891–896 (1966)

Cook, G.E.: Luni-solar perturbations of the orbit of an earth satellite. Geophys. J. **6**(3), 271–291 (1962)

Efroimsky, M., Goldreich, P.: Gauge freedom in the N-body problem of celestial mechanics. Astron. Astrophys. **415**, 1187–1199, astro-ph/0307130 (2004)

Efroimsky, M.: Long-term evolution of orbits about a precessing oblate planet. 1. The case of uniform precession. astro-ph/0408168 (2004) [This preprint is a very extended version of Efroimsky (2005)]

Efroimsky, M.: Long-term evolution of orbits about a precessing oblate planet: 1. The case of uniform precession. Celestial Mech. Dynam. Astron. **91**, 75–108 (2005)

Efroimsky, M.: Long-term evolution of orbits about a precessing oblate planet: 2. The case of variable precession. Celestial Mech. Dynam. Astron. **96**, 259–288 (2006a)

Efroimsky, M.: Long-term evolution of orbits about a precessing oblate planet: 2. The case of variable precession. astro-ph/0607522 (2006b) [This preprint is a very extended version of Efroimsky (2006a)]

Efroimsky, M.: Gauge freedom in orbital mechanics. Ann. N. Y. Academy Sci. **1065**, 346–374, astro-ph/0603092 (2006c)

Efroimsky, M., Lainey, V.: The physics of bodily tides in terrestrial planets, and the appropriate scales of dynamical evolution. J. Geophys. Res.—Planets (2007, in press)

Everhart, E.: An efficient integrator that uses Gauss-Radau spacings. Dynamics of comets: their origin and evolution. In: Carusi, A., Valsecchi, G.B. (eds.) Proceedings of IAU Colloquium 83 held in Rome on 11–15 June 1984. vol. 115, p. 185. Astrophysics and Space Science Library, Dordrecht, Reidel (1985)

Goldberg, D.E.: Genetic Algorithms in Search, Optimization and Machine Learning. Addison-Wesley, Reading, MA (1989)

Goldreich, P.: Inclination of satellite orbits about an oblate precessing planet. Astron. J. **70**, 5–9 (1965)

Gurfil, P., Kasdin, N.J., Arrell, R.J., Seager, S., Nissanke, S.: Infrared space observatories: How to mitigate zodiacal dust interference. Astrophys. J. **567**, 1250–1261 (2002)

Gurfil, P., Kasdin, N.J.: Characterization and design of out-of-ecliptic trajectories using deterministic crowding genetic algorithms. Comput. Methods Appl. Mech. Eng. **191**, 2169–2186 (2002a)

Gurfil, P., Kasdin, N.J.: Niching genetic algorithms-based characterization of geocentric orbits in the 3D elliptic restricted three-body problem. Comput. Methods Appl. Mech. Eng. **191**, 5673–5696 (2002b)

Hartmann, W.K.: Martian cratering 9: toward resolution of the controversy about small craters. Icarus **189**, 274–278 (2007)

Innanen, K.A., Zheng, J.Q., Mikkola, S., Valtonen, M.J.: The Kozai Mechanism and the stability of planetary orbits in binary star systems. Astron. J. **113**, 1915–1919 (1997)

Kilgore, T.R., Burns, J.A., Pollack, J.B.: Orbital evolution of "Phobos" following its "capture". Bull. Am. Astron. Soc. **10**, 593 (1978)

Kozai, Y.: On the effects of the Sun and the Moon upon the motion of a close Earth satellite. SAO Special Report **22**, 7–10 (1959)

Kozai, Y.: Effect of precession and nutation on the orbital elements of a close earth satellite. Astron. J. **65**, 621–623 (1960)

Lainey, V., Duriez, L., Vienne, A.: New accurate ephemerides for the Galilean satellites of Jupiter. I. Numerical integration of elaborated equations of motion. Astron. Astrophys. **420**, 1171–1183 (2004)

Lainey, V., Gurfil, P., Efroimsky, M.: Long-term evolution of orbits about a precessing oblate planet: 4. A comprehensive model (2008 in preparation)

Laskar, J.: Secular evolution of the solar system over 10 million years. Astron. Astrophys. **198**, 341–362 (1988)

Laskar, J., Robutel, J.: The chaotic obliquity of the planets. Nature **361**, 608–612 (1993)

Murison, M.: Satellite Capture and the Restricted Three-Body Problem. Ph.D. Thesis, University of Wisconsin, Madison (1988)

Nesvorný, D., Vokrouhlický, D.: Analytic theory of the YORP effect for near-spherical objects. Astron. J. **134**, 1750–1768 (2007)

Paige, D.A., Golombek, M.P., Maki, J.N., Parker, T.J., Crumpler, L.S., Grant, J.A., Williams, J.P.: MER small-crater statistics: evidence against recent quasi-periodic climate variations. Seventh Int. Conference Mars, 9–13 July 2007, Caltech, Pasadena, CA (2007)
Pang, K.D., Pollack, J.B., Veverka, J., Lane, A.L., Ajello, J.M.: The composition of phobos: evidence for carbonateous chondrite surface from spectral analysis. Science **199**, 64 (1978)
Pollack, J.B., Burns, J.A., Tauber, M.E.: Gas drag in primordial circumplanetary envelopes. a mechanism for satellite capture. Icarus **37**, 587 (1979)
Proskurin, V.F., Batrakov, Y.V.: Perturbations of the motion of artificial satellites, caused by the earth oblateness. Bull. Inst. Theor. Astro. **7**, 537–548 (1960)
Smith, D.E., Lemoine, F.G., Zuber, M.T.: Simultaneous estimation of the masses of mars, phobos, and deimos using spacecraft distant encounters. Geophys. Res. Lett. **22**, 2171–2174 (1995)
Szebehely, V.: Theory of Orbits. Academic Press, NY (1967)
Tolson, R.H., 15, collaborators.: Viking first encounter of phobos. Preliminary results. Science **199**, 61 (1978)
Touma, J., Wisdom, J.: The chaotic obliquity of Mars. Science **259**, 1294–1297 (1993)
Touma, J., Wisdom, J.: Lie-Poisson integrators for rigid body dynamics in the solar system. Astron. J. **107**, 1189–1202 (1994)
Veverka, J.: Phobos and deimos. Sci. Am. **236**, 30 (1977)
Ward, W.: Large-scale variations in the obliquity of Mars. Science **181**, 260–262 (1973)
Ward, W.: Climatic variations of Mars. Astronomical theory of insolation. J. Geophys. Res. **79**, 3375–3386 (1974)
Ward, W.: Present obliquity oscillations of Mars—Fourth-order accuracy in orbital e and i. J. Geophys. Res. **84**, 237–241 (1979)
Ward, W.: Comments on the long-term stability of the earth's obliquity. Icarus **50**, 444–448 (1982)
Zhang K., Hamilton, D.P.: Dynamics of inner neptunian satellites. Abstracts of the 37th DPS Meeting of the Americal Astronomical Society. In: AAS Bulletin, **37**, 667–668 (2005)
Waz, P.: Analytical theory of the motion of phobos: a comparison with numerical integration. Astron. Astrophys. **416**, 1187–1192 (2004)